# Modeling of the intrinsic softening of $\gamma$-carbides in cemented carbides

V. Lamelas, L. Tian, Manon Rolland, M. Walbrühl, R. Lizárraga, A. Borgenstam

Materials Today Communications 37 (2023) 107454

Contents lists available at ScienceDirect

Materials Today Communications

journal homepage: www.elsevier.com/locate/mtcomm

# Modeling of the intrinsic softening of γ-carbides in cemented carbides

V. Lamelas [a,*], L. Tian [a], M. Bonvalet-Rolland [a,b], M. Walbrühl [c], R. Lizárraga [a], A. Borgenstam [a]

[a] KTH Royal Institute of Technology, Department of Materials Science and Engineering, Brinellvägen 23, SE-100 44 Stockholm, Sweden
[b] UMET, Unité Matériaux et Transformations, Université de Lille, CNRS, INRAe, Centrale Lille, UMR 8207, 59000 Lille, France
[c] AB Sandvik Coromant R&D, Lerkrogsvägen 19, SE-126 80 Stockholm, Sweden

ARTICLE INFO

*Keywords:*
Cemented carbides
Hardness
Transition metal carbides
First principles
Modelling
Peierls-Nabarro

ABSTRACT

Cemented carbides are widely used materials in industrial applications due to their remarkable combination of hardness and toughness. However, they are exposed to high temperatures during service leading to a reduction of their hardness. A common practice to damp this softening is to incorporate transition metal carbides in cemented carbide compositions, which keeps the hardness relatively higher when temperature increases. Understanding the underlying mechanisms of this softening is crucial for the development of cemented carbides with optimal properties. In this work, atomic-scale mechanisms taking place during plastic deformation are analyzed and linked to the effect that they have on the intrinsic macro-scale softening of the most common TMC used in cemented carbides grades (TiC, ZrC, HfC, VC, NbC and TaC). The proposed model uses the generalized stacking fault energy obtained from density functional theory calculations as an input to Peierls-Nabarro analytical models to obtain the critically resolved shear stress needed for deformation to occur in different slip systems. Subsequently, this information is used to predict the hardness variation across the temperature service range experienced by cemented carbides in wear applications.

In addition to the prediction of hot-hardness for TMC, the obtained results also offer valuable insights into the intrinsic mechanisms governing TMCs deformation. The results facilitate the identification of dominant dislocation types influencing plasticity within distinct temperature regimes, define energetically favorable slip systems, and predict the brittle-ductile transition temperature in these materials. For instance, for group IV carbides at low temperatures, the slip system with a lower GSFE is $\{110\} < 1\bar{1}0 >$ and around 30% of their melting temperature, the GSFE of partial slip in $\{111\} < 1\bar{2}1 >$ becomes lower, changing the dominant slip mechanism and characterizing the Brittle-Ductile transition.

## 1. Introduction

Cemented carbides are widely used materials due to their remarkable combination of hardness and toughness. When in operation, cemented carbide components face high levels of pressures and can reach flash temperatures as high as 1200 °C [1]. These conditions cause a reduction in the material's hardness, which negatively impacts its performance. The softening of cemented carbides within the operational temperature range is characterized by three well-defined regions with distinct mechanical behavior. Each region's onset is determined by the activation of characteristic mechanisms acting simultaneously at different length-scales and phases. At moderately low temperatures (from room temperature to approximately 450–500 °C) and high temperatures (above 850 °C), relaxation mechanisms in the binder predominantly influence the mechanical behavior of cemented carbides. In the intermediate temperature range, macroscopic softening is driven by relaxation mechanisms activated within the hard phases [2]. At this temperature range, the dislocation mobility in the carbides is activated through a Peierls-Nabarro (P-N) mechanism, and the contribution of the carbide's strain on macroscopic deformation becomes significant.

The addition of transition metal carbides (TMC), known as γ-carbides, in cemented carbide compositions has empirically proven to be advantageous in maintaining higher hot hardness over a broader temperature range. However, the precise mechanisms responsible for this improvement remain not fully understood [3]. It can be attributed to TMC having high intrinsic hardness that contribute positively to the hot hardness of cemented carbides, as well as reducing the extent of higher-scale mechanisms such as grain boundary sliding acting at higher temperatures. To distinguish the contribution of these effects, it is considered relevant to first accurately model the intrinsic softening of

* Corresponding author.
*E-mail address:* vlc@kth.se (V. Lamelas).

https://doi.org/10.1016/j.mtcomm.2023.107454
Received 19 October 2023; Accepted 27 October 2023

TMC at intermediate temperatures. The present work proposes a model that describes the intrinsic softening of TMC present in cemented carbides, with a special focus on the P-N mechanism that allows carbides to deform.

The mechanical behavior of TMC is significantly affected by temperature and strain rate [4,5], and can be segmented into four stages approximately defined by characteristic homologous temperatures of the carbide:

- From room temperature to 0.3 times the melting temperature ($T_m$) (about 1000 K for TiC), dislocation movement is governed by their intrinsic mobility, which is characterized by a high intrinsic lattice friction. This means that plastic deformation requires very high critical resolved shear stresses (CRSS) and strong thermal activation.
- From $0.3{\cdot}T_m$ to $0.46{\cdot}T_m$ (about 1550 K for TiC), the thermal activation is high enough to overcome lattice friction and plastic shear is slightly affected by temperature or strain rate. Ductility in this range is governed by the dislocations surmounting long-range stress fields caused by other dislocations [6].
- From $0.46{\cdot}T_m$ to $0.66{\cdot}T_m$ (about 2200 K for TiC), the creep region starts, and ductility is then governed by diffusion of the interstitial atoms, C and/or N.
- From $0.66{\cdot}T_m$, bulk diffusion of metal atoms becomes relevant and dominates plasticity.

Multiple studies have been conducted to understand the fundamental mechanisms involved in the Brittle-Ductile (B-D) transition of TMC. The main consensus is that the mechanical transition is correlated with the activation of additional slip planes, but the specific conditions leading to such activation remain unclear [7–14]. What is certain is that the characteristics of the dominant slip system will strongly impact the material's macroscopic properties. Therefore, for the modelling efforts presented here, a good understanding of the ruling slip systems at every temperature range becomes essential to incorporate the B-D transition into the current model.

TMC have a rock salt B1 crystal structure that can be considered as two FCC interpenetrating lattices of substitutional atoms and interstitial atoms, the former occupying the octahedral interstices. Inherent to their crystallography, the available close packed slip direction is $<1\bar{1}0>$in {100}, {110} and {111} planes. The $\{100\}<1\bar{1}0>$and $\{110\}<1\bar{1}0>$slip families contain 6 planes and 1 slip direction per plane, resulting in only 2 independent slip systems. Conversely, the $\{111\}<1\bar{1}0>$slip family, contains 4 planes and 3 slip direction per plane [15]. Despite sharing the same crystallographic symmetry and bonding nature, group IV (TiC, ZrC, HfC) and group V (VC, NbC, TaC) TMC present different slip behavior and therefore different mechanical properties [16].

The first assessments of the slip systems involved in TMC plasticity used hardness anisotropy testing (HA) to infer the dominant activated slip systems [17–21]. These studies showed significant slip differences at room temperature between two TMC representatives of groups IV and V (HfC and TaC, respectively). The preferred slip system was {110} for HfC, and {111} for TaC. This difference leads to a clear impact on the ductility of the materials since $\{110\}<1\bar{1}0>$slip systems do not have the 5 independent slip systems needed to fulfill Von Mises Criterion, as {111} planes do. These studies were extended to higher temperatures [17] and activation of {111} planes in group IV carbides was then observed.

This difference and changes in dominant slip systems are known since the early 70 s, and further micromechanical testing [22,23] or direct transmission electron microscopy (TEM) observations [7,9,16, 23–25] have confirmed their validity. However, these studies have also added some uncertainty since many times both slip systems are found to be active simultaneously and occasionally even slip in the {100} plane has been observed [23]. The diversity of observed slip systems dependent on the loading conditions (stress system, strain rate, and plastic onset) or material stoichiometry shows the complexity of attempting to identify empirically a single slip system ruling the plasticity of TMC. Therefore, the determination of the dominant slip systems by means of theoretical methods relying on intrinsic characteristics of the materials structure becomes very valuable.

The use of density function theory (DFT) calculations has provided a more accurate and fundamental understanding of slip in TMC [16, 26–28]. De Leon [16] calculated the generalized stacking fault energies (GSFE) using DFT for $\{110\}<1\bar{1}0>$and $\{111\}<1\bar{1}0>$slips at 0 K, proving that {110} slip is more energetically favorable than {111} for group IV and group V carbides. This also results in a lower CRSS required for slip to occur. The GSFE was systematically higher for group IV carbides than for their group V counterparts, partly explaining the higher ductilities observed experimentally for group V. Further, DFT calculations showed that group V carbides have an intrinsic stacking fault (ISF) in the $\{111\}<1\bar{2}1>$ slip system that allows the splitting of dislocation into partials, making the slip through this slip system favorable despite being energetically unfavorable with respect to $\{110\}<1\bar{1}0>$slip. The findings by De Leon highlight the second most important factor, after the dominant slip plane, affecting the B-D transition in TMCs, namely the slip-controlling mechanism and the dislocation character i.e. partial-perfect or screw-edge-mixed [29].

In this work the advantages of analyzing the contribution of each slip system using theoretical methods are highlighted and extended to consider the effect of finite temperatures. The considered temperature range is limited to that applicable to metal cutting or machining (up to 1450 K), thus, mechanisms acting at higher temperatures such as carbon diffusion or metal vacancy diffusion are out of the current scope. The sole relevant mechanism at such temperature range is the P-N mechanism, which can be described by means of P-N based models. These models consider a dislocation lying between two discrete atomic planes that define the Peierls potential periodicity (typically a sinusoidal-like periodic function). Above and below these facing planes, the material is approximated as a continuum medium [30,31]. The continuous distribution of shear that this dislocation introduces in the material lattice is known as the dislocation misfit or disregistry. The magnitude of the distortion introduced in the perfect lattice is determined by the Burgers vector, $b$, of the dislocation, being $b/2$ at its center. The rest of the introduced distortion propagates along the crystal lattice in a higher or lower extent depending on several factors including the crystal periodicity, elastic properties or dislocation character. Usually, this disregistry is described by a trial function that varies in complexity and that can be physically thought of as a set of discrete partial dislocations.

The CRSS needed to move a dislocation along the P-N potential, is then obtained by relating the energy introduced by this disregistry or shear along the glide plane with the restoring force acting on both sides of the interface when the dislocation slips. The simplest form to express this balance is:

$$\frac{\tau_c}{G} = C \bullet \frac{b}{\delta} \bullet \exp\left(-A \bullet \frac{d}{\delta}\right) \tag{1}$$

where $\tau_c$ is the shear stress at which the dislocation glides, $G$ is the shear modulus, $\delta$ is the period of the Peierls potential, $d$ is the spacing between gliding planes, and $A$ and $C$ are constants that depend on the materials Poisson ratio and the dislocation character (Screw/Edge, Perfect/Partial) [31].

In materials such as TMC, where atomic bonding has a strong covalent character, dislocations do not slip as a whole from one potential valley to the next one. Instead, they advance through kink pairs, where first a segment of critical length jumps into the next valley due to thermal fluctuations. And second, the rapid lateral motion of the kinks brings the dislocation line to the next low-energy position. The dislocation velocity is determined by the rate of formation of kink pairs along straight dislocation segments lying in the Peierls potential valleys [29].

The constitutive equation that overcomes the complexity of considering atomistic simulations to determine the dislocation velocity was given by Hirth and Lothe (H-L) [32] as:

$$v = \nu_D \bullet \tau \bullet \frac{abh^2}{k_B T} \bullet \exp\left(-\frac{W_m}{k_B T}\right) \tag{2}$$

where $\nu_D$ is the Debye frequency, $\tau$ is the resolved shear stress on the dislocation, $k_B T$ are Boltzmann constant and temperature; $a$ and $h$ are the lattice parameter and kink height respectively, which define the Peierls potential periodicity; and $W_m$ is the activation-energy barrier for kink motion.

Classical work from Hirth and Lothe [31] has suggested combining the P-N energy balance resulting from a dislocation gliding on a given plane; the kink-pair formalism that rules dislocation gliding kinetics; and the Orowan relation [33] to model creep and constant strain-rate deformation processes resulting in:

$$\frac{\tau_c^T}{G} = C_1\left[C_2 \bullet \ln\left(C_3\frac{G}{\tau_c^T}\right) - \frac{k_B T}{a^3 G}\ln\left(\frac{\rho_m b \lambda_b \nu_D}{\dot{\varepsilon}}\right)\right]^2 \tag{3}$$

where $\tau_c^T$ is the critical shear for dislocation slip at a given temperature, $\rho_m$ is the dislocation density, $\lambda_b$ in the mean free path of dislocations slipping over obstacles and $\dot{\varepsilon}$ is the strain rate. $C_1$, $C_2$ and $C_3$ are of high relevance and are dependent on the slip system and dislocation character, and are defined as:

$$C_1 = \frac{2\pi a^6}{h^3 b^3 A_2} \tag{4}$$

$$C_2 = \frac{hb^2 A_1}{4\pi a^3} \tag{5}$$

$$C_3 = \frac{hbA_2}{8\pi r^2} \tag{6}$$

where $r$ is the dislocation core radius and $A_1$and $A_2$ are geometric constants that depend on the dislocation character defined as:

$$A_1 = \cos^2\beta + \frac{\sin^2\beta}{1-\nu} \tag{7}$$

$$A_2 = \frac{(1+\nu)\cos^2\beta + (1-2\nu)\sin^2\beta}{1-\nu} \tag{8}$$

where $\nu$ is the Poisson ratio and $\beta$ is the angle between the dislocation line and the Burgers vector.

In this work, Eq. 3 is adapted to the particular case of TMC up to homologous temperatures of $0.46{\cdot}T_m$. In Section 2, we present the considerations taken to move from CRSS to macroscopic hardness and we describe our approach to adapt Eq.3 to model TMC's. The results of the modelling scheme are described in Section 3 and are compared to experimental data in Section 4 where also the ruling slip systems and involved mechanisms are discussed in detail.

## 2. Modeling approach

In the current approach the plasticity of TMCs is predominantly attributed to dislocation slipping and the motion of other crystal defects such as vacancies (0D), and grain or twin boundaries (2D) are not considered. Dislocation slip is activated (material reaches its yield point) when the resolved shear stress (RSS) on a given plane reaches a critical value CRSS. The RSS, $\tau_{RSS}$, is related to the applied stress through the Schmid's Law [34], which decomposes a certain stress configuration acting on a plane through the following geometric relation:

$$\tau_{RSS} = \cos\lambda \bullet \cos\theta \bullet \sigma = m \bullet \sigma, \tag{9}$$

where $\sigma$ is the applied stress, $\lambda$ is the angle between the normal of the slip plane and the direction of the applied stress, $\theta$ is the angle between the slip direction and the applied stress direction, and $m$ is the Schmid factor. At this point, a good empirical relation that can be used to relate yield stress, $\sigma_y$, to hardness, $H$, is Tabor's relation [35], which is expressed as

$$H = \alpha \bullet \sigma_y, \tag{10}$$

where α is a constraint factor that only depends on the geometry of the indenter. However, Tabor relation assumes a fully work hardened isotropic material in which elastic deformation can be dismissed. Further work [36], extended this relation to materials where elasticity needs to be considered, such as carbides, reaching the following modified constraint factor:

$$\alpha = \frac{2}{3}\left[\frac{1+\ln(E \bullet \cos(\varphi))}{3 \bullet \sigma_y}\right], \tag{11}$$

where $E$ is the young modulus of the indented material and $\varphi$ is the semi-angle of the indenter (being 68° for Vickers testing). Therefore, combining the modified Tabor and the Schmid equations, and using Eq. 3, the hardness can be modeled as a function of temperature for every slip system $i$ as (see Fig. 1):

$$H(T)_i = \alpha_i \bullet \frac{\tau_c^T i}{m_i}. \tag{12}$$

Hardness relies on the measurement of the indent left after loading with the indenter. Hence, the material needs to be plastically deformed in order to leave an indentation that can be measured. Even in brittle materials, the high hydrostatic pressures developed under the indentation inhibit the brittle failure, and hardness testing is essentially a measure of the plastic properties of the material [37]. Because of this, the slip systems that are considered to determine the hardness are those fulfilling Von Misses criterion i.e., the ones belonging to the {111} plane. For the specific case of dislocations in the {110} plane, their slip contributes to the dislocation-dislocation interaction, but their contribution to the deformation of the material can be considered negligible. In the current approach, the contribution of each slip system causing deformation is weighted so that the slip system with a lower CRSS contributes to a higher extent to the deformation. For instance, if two slip systems have the same CRSS, their contribution to the total hardness will be equal. The chosen weighting equation can be written as:

$$H_{TOT} = \sum_{i \neq j} H(T)_i \bullet \frac{\prod H(T)_j}{\prod H(T)_j + \sum H(T)_j \bullet H(T)_i}. \tag{13}$$

Fig. 1 shows the integrated workflow followed for the determination of hardness of TMC as a function of temperature. The correct description of the macroscopic hardness of TMC relies on the correct modeling of mechanisms acting at lower scales, such as atomic/micro-scales, and translating their effect to the relevant properties of polycrystalline materials. It applies for instance to the treatment of the Schmid factor, see Fig. 1. To extrapolate low-scale results to the behavior of polycrystalline materials, all possible combinations of relative orientation between applied stress and the relevant slip planes are considered to occur under indentation conditions. Based on this, and to keep the modelling simple, a mean value for the Schmid factor is calculated and used in the same way as a Taylor orientation factor is used when determining the yield stress of polycrystalline materials from their CRSSs [38]. The Schmid factor for $\{110\} < 1\bar{1}0 >$, $\{111\} < 1\bar{1}0 >$and $\{111\} < 1\bar{2}1 >$slip systems has been reported as a function of crystallographic orientation for $\lambda = 45°$ [22]. Averaging all possible orientation combinations, the resultant $m_i$ constants are 0.24, 0.39 and 0.35 respectively for $\{110\} < 1\bar{1}0 >$, $\{111\} < 1\bar{1}0 >$and $\{111\} < 1\bar{2}1 >$.

From Eq. 12 it is thus clear that the main factor affecting the modeled hardness is the CRSS. Fig. 1 schematically depicts how the main factors affecting the CRSS in Eq. 3 are obtained and where in the equation are

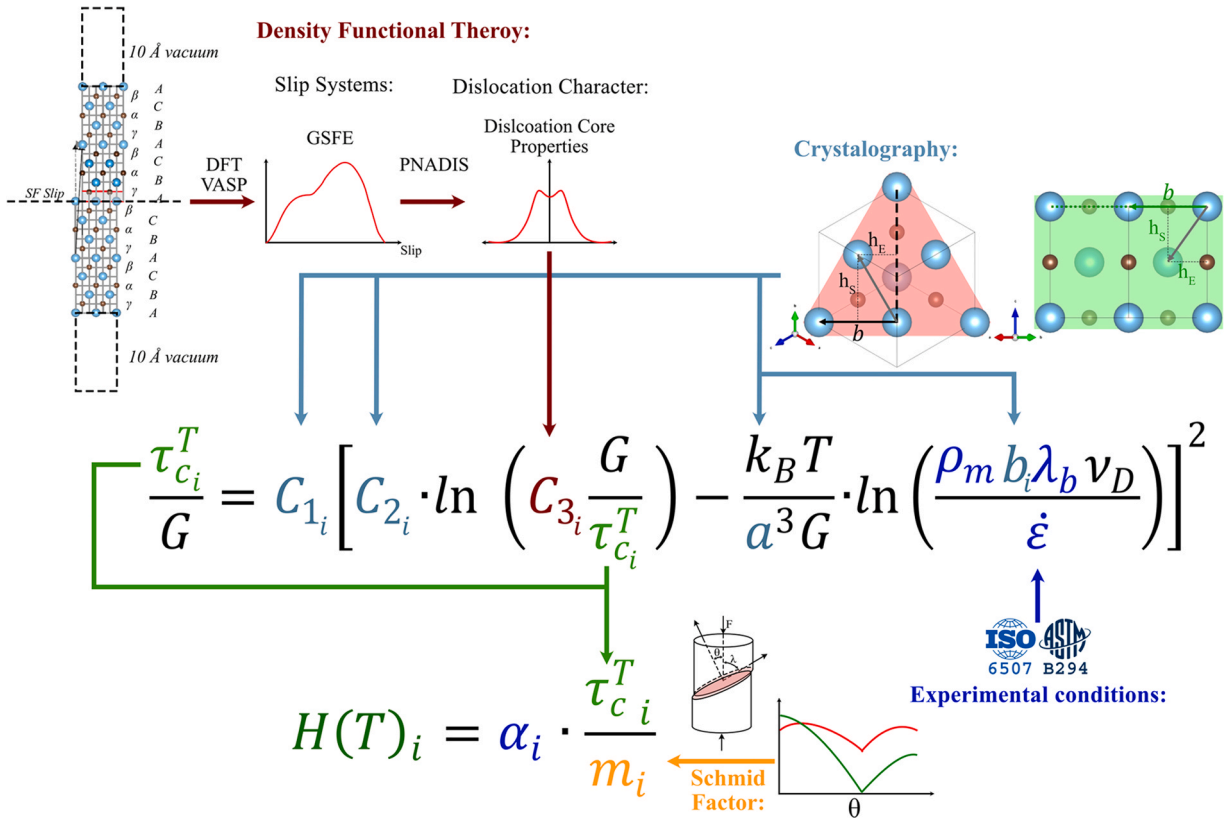


**Fig. 1.** Workflow followed for the determination of the hot hardness of carbides. (2-column fitting image).

acting. It can be observed that the main factors affecting the CRSS are the operative slip system, the dislocation character, the elastic constants of the material, and the experimental conditions in order of relevance. A detailed description of how each of these factors have been considered in the modeling of TMC's hardness is presented in the following sections.

### 2.1. Slip systems

*Ab initio* calculations of the GSFE at 0 K along the slip directions of TMC have proven to be a very valuable tool to explain the differences between group IV and group V carbides [26; 16]. In these calculations, a perfect crystal is slipped along the direction of interest, and the surplus energy that the slipped configuration has over the perfect lattice per unit area can be interpreted as an interfacial restoring stress. According to Vitek [39], this restoring stress shares the same physical interpretation as the restoring force in the P-N model. Given this relation and considering the significant effect of temperature on experimental observations, it is of interest to investigate how the characteristic GSFE for each slip family evolves with temperature. For such purpose, the GSFE of TiC and VC, as representatives of group IV and group V carbides, are computed here by means of density functional perturbation theory (DFPT) [40] including temperature effects at harmonic level. Free energies including phonon contributions are obtained within the framework of DFPT as implemented in the Vienna ab initio simulation package (VASP), which is based in the projector augmented waves approach (PAW) [41]. The exchange-correlation functional was described using the Perdew, Burke, and Ernzerhof (PBE) parametrization [42].

Firstly, the B1 unit cell of TiC and VC were relaxed, and the equilibrium lattice constants of 4.34 Å and 4.16 Å were obtained for each system, respectively. Secondly, the GSFE at 0 K for $\{111\} < 1\bar{2}1 >$and $\{110\} < 1\bar{1}0 >$slips considering lattice relaxation effects were calculated. 15 and 10 displacement supercells were created for $\{111\} < 1\bar{2}1 >$and $\{110\} < 1\bar{1}0 >$slips, respectively. Each supercell contained 24 layers (96 atoms), and the atomic positions were relaxed along the Z-axis by minimizing the forces to less than 0.03 eV/Å on each atom. Internal convergence parameters were carefully checked so that total energy differences were below $10^{-5}$ eV. A cutoff energy of 600 eV was used. For the GSFE calculations, a 9 × 9 × 1 with gamma-centered scheme of k-points was used. A vacuum width of 20 Å was added to periodical slabs for all configurations (See Fig. 1). Lastly, the phonon contribution calculation with temperatures between 0 and 1400 K was performed using the open-source package Phonopy available in VASP [43,44].

The total free energy at a finite temperature is calculated as:

$$F(T) = E_0 + F_{vib}(T) \tag{14}$$

where $E_0$ corresponds to the internal energy at 0 K, and $F_{vib}(T)$ is the phonon contribution to the free energy. The GSFE or $\gamma_{SF}$ corresponding to different sheared configurations along a particular direction at finite temperature is calculated by using the following expression:

$$\gamma_{SF}(b,T) = \frac{F_{fault}(b,T) - F_{perfect}(T)}{A(T)} \tag{15}$$

where $F_{fault}(b,T), F_{perfect}$ *and* $A(T)$ correspond to the free energy of the sheared lattice, free energy of the perfect fcc structure and the area of the supercell basal plane (slip plane), respectively. Special attention has been given to the $\{111\} < 1\bar{2}1 >$slip in group IV carbides, where DFT calculations can provide valuable insights on the possibility of formation of an ISF [26], as well as determining the temperature at which it becomes energetically favorable. This information can further be used in partially explaining the B-D transition observed in the experiments [21]. As discussed above, many slip systems can coexist during a mechanical test. For a polycrystalline material all the possible slip systems can be activated and should be considered, depending on the orientation relations. In this regard, the description of the material's mechanical

behavior benefits from considering a variety of dislocation types and slip systems. Therefore, the resolved shear stresses for all dislocation characters in planes {111} and {110} are calculated for group IV and V TMCs and accounted for in the modeling of the hardness.

### 2.2. Dislocation character

In the current modeling approach, the dislocation character is described through the constants $C_1$, $C_2$, and $C_3$ in Eqs. 4 to 6. On one hand, constants $A_1$ and $A_2$ are defined based on the relative angle between the dislocation line and the burgers vector, ranging from 0° to 90°. In this work edge (90°), screw (0°) and mixed (30°, 60°) character dislocations are considered for the entire range of temperatures and stresses. The Burgers vector ($b$) and P-N energy field periodicity ($h$) are directly determined from the lattice crystallography. $b$ is calculated in the usual way, while $h$ is defined as the minimum value of the projection of the lattice translation vectors on top if the slip plane to the perpendicular of the dislocation line [30]. Table 1 summarizes the values obtained for all dislocations considered in this study.

On the other hand, the determination of the core radius, $r$, does not depend exclusively on crystallographic relations and its exact definition is more complex. The dislocation core refers to the central region of the dislocation line where the misalignment is the most severe, but there is no unique way to establish where the dislocation core finishes, and the purely elastic field starts [25,45]. Additionally, the atomic-level determination of the dislocation core structure in ceramics is computationally very heavy, and that becomes even more complex when stoichiometry or polymorph variants are considered [46]. Nevertheless, the calculated values of CRSS are very sensitive to the half-width of the dislocation, making an accurate definition of this parameter crucial. In consequence, two different methods for defining the dislocation core radius using the P-N model framework are evaluated and discussed here.

Both methods for defining $r$ involve solving the P-N equation that relates disregistry with the restoring force acting on both sides of the slipped lattice. In both methodologies, the relation between the restoring force and GSFE established by Vitek [39] is used. When the change of the SFE with slip is relatively steep, the restoring forces acting across the interface are large, which confine the dislocation core to smaller widths. Technically, the GSFE curve obtained through ab initio calculations is derived with respect to the displacement and made equivalent to the restoring force. Then, a least square minimization of the difference between the elastic resistance caused by the shear and the recovery force is performed. In the first methodology [47], hereafter referred to as analytical, the trial function used to describe the disregistry assumes that the restoring force has a sinusoidal form, and it is mostly determined by the maximum resolved shear stress at maximum SFE. The analytical expression for the dislocation half width (ξ) is:

$$\xi = \frac{Kb}{4\pi\tau_{\max}} \tag{16}$$

On the other hand, the second methodology does not assume a purely sinusoidal function for the restoring force and disregistry, but instead describes them as a sine and arctan series [48] [48], further considering the shape of the GSFE and not only its maximum value. In the current work, if the GSFE has a single maximum, the disregistry series function is developed up to the third order, and for those with two maximums, sixth order is used. In this method, hereafter referred to as Disregistry-based, the dislocation half width is defined as half of the atomic distance over which the disregistry changes from $\frac{1}{4}b$ to $\frac{3}{4}b$ (See Fig. 2).

In the present study, the core size ($r$) has been approximated to be equivalent to the dislocation half width calculated as previously described. Technically, the computation of the dislocation half-width was performed using PNADIS open source software [49] and input from ab initio GSFE taken from literature [26] and the present study.

**Table 1**
Crystallographic and dislocation character defining parameters.

| Slip Plane | Slip Direction | Screw / Edge | β | b | h |
|---|---|---|---|---|---|
| {1 1 0} | $\frac{1}{2}<1\bar{1}0>$ | S | 0° | $\frac{a}{\sqrt{2}}$ | $\frac{a}{2}$ |
| | | E | 90° | | $\frac{a}{2\sqrt{2}}$ |
| {1 1 1} | $\frac{1}{2}<1\bar{1}0>$ | S | 0° | $\frac{a}{\sqrt{2}}$ | $\frac{\sqrt{6}a}{4}$ |
| | | E | 90° | | $\frac{a}{2\sqrt{2}}$ |
| | $\frac{1}{6}<1\bar{2}1>$ | Mix | 30° | $\frac{a}{\sqrt{6}}$ | $\frac{\sqrt{6}a}{4}$ |
| | | Mix | 60° | | |

**Table 2**
Elastic constants and lattice parameter as function of temperature as obtained in Ref. [46] and Ref. [50].

| | G (x10$^9$) | B (x10$^9$) | a (T) (m) |
|---|---|---|---|
| TiC | $-1.24\bullet10^{-5}\bullet T^2+177.12$ | $-2.17\bullet10^{-5}\bullet T^2+274.43$ | $4.297\bullet10^{-10}\bullet(1+T\bullet8.0\bullet10^{-6})$ |
| ZrC | $-1.31\bullet10^{-5}\bullet T^2+164.69$ | $-1.81\bullet10^{-5}\bullet T^2+229.71$ | $4.666\bullet10^{-10}\bullet(1+T\bullet7.6\bullet10^{-6})$ |
| HfC | $-8.33\bullet10^{-6}\bullet T^2+178.02$ | $-1.79\bullet10^{-5}\bullet T^2+259.37$ | $4.606\bullet10^{-10}\bullet(1+T\bullet7.0\bullet10^{-6})$ |
| VC | $-2.39\bullet10^{-5}\bullet T^2+205.91$ | $-3.99\bullet10^{-5}\bullet T^2+324.42$ | $4.122\bullet10^{-10}\bullet(1+T\bullet8.9\bullet10^{-6})$ |
| NbC | $-2.83\bullet10^{-5}\bullet T^2+197.30$ | $-1.25\bullet10^{-5}\bullet T^2+298.15$ | $4.479\bullet10^{-10}\bullet(1+T\bullet7.8\bullet10^{-6})$ |
| TaC | $-2.62\bullet10^{-5}\bullet T^2+233.67$ | $-2.72\bullet10^{-5}\bullet T^2+339.09$ | $4.440\bullet10^{-10}\bullet(1+T\bullet7.5\bullet10^{-6})$ |

### 2.3. Elastic constants and lattice parameters

The current methodology requires the elastic constants as a function of temperature to calculate the hot hardness of the evaluated TMCs. The shear modulus and lattice parameter for TiC, ZrC, HfC, VC and TaC are obtained from reference [46] from ab initio molecular dynamics simulations, while for NbC, they are obtained from experiments [50]. For the extrapolation of elastic constants at temperatures higher than reported, 2-nd order polynomial fitting, imposing a null slope at T = 0 K, was used.

Poisson ratio is calculated for each temperature using continuum

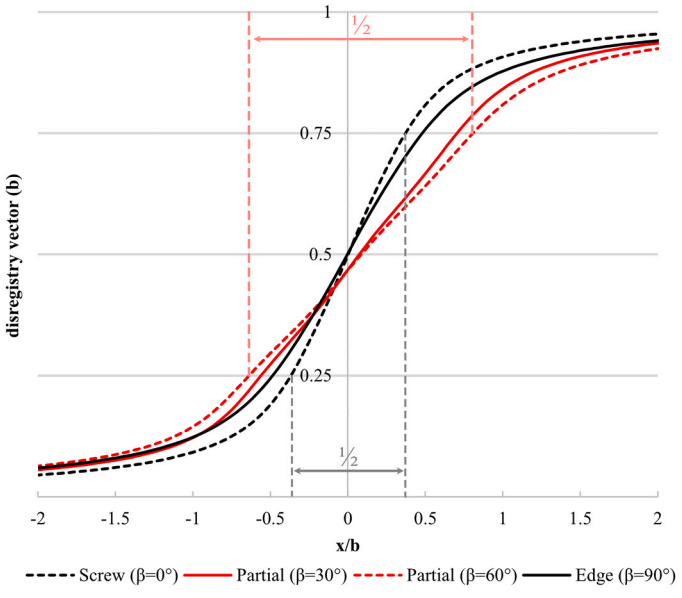


**Fig. 2.** Disregistry vector in burgers vector units obtained from DFT GSFE treatment for screw, 30,60 and edge dislocation for TiC in the {111} plane. (single column fitting image).

mechanics, leading to the following relation:

$$\nu(T) = \frac{3B(T) - 2G(T)}{6B(T) + 2G(T)} \tag{17}$$

### 2.4. Experimental and material conditions

The second logarithm in Eq. 3 is shown to be dependent on the experimental conditions, specifically the strain rate ($\dot{\varepsilon}$) and the dislocation density of the tested crystal, which determine the density of mobile dislocations ($\rho_m$) and the mean free path between sessile dislocations ($\lambda_b$). Since the current modeling is limited to the description of hardness, the strain rate is considered to be restricted to that imposed by loading conditions defined in hardness testing. Although the strain rate along a single indentation is not uniform, it starts by having high values and decreases gradually as the area resisting the indenter increases [51]. Nonetheless, an average indentation strain rate ranging from $10^{-5}$ to $10^{-3}\,s^{-1}$ can be calculated for Vickers tests [52]. For the specific case of TMC, the indentation strain rate is usually considered to be closer to the higher values [53], and therefore a strain rate of $10^{-3}\,s^{-1}$ is adopted in this study.

The Debye frequency for each carbide has been calculated using its relation to the Debye temperature:

$$\nu_D = \frac{k_B}{\hbar}\theta_D, \tag{18}$$

where, $\hbar$ is the reduced Plank constant and $\theta_D$ is the Debye temperature taken from ref. [54].

$\rho_m$ and $\lambda_b$ are influenced by processing conditions, temperature, strain level and the applied shear stress. Since the shear stress acting on the dislocation is the desired quantity from computation, $\rho_m$ and $\lambda_b$ cannot be known a priori. Thus, their product will be treated as a adjusting parameter (referred to as DDL) with its value ranging within the common values found in the specific case of TMCs inside of cemented carbides. Based on the literature-reported values, the range of mobile dislocation densities is expected to be between $2.29 \bullet 10^{16}$ and $2.60 \bullet 10^{9} m^{-2}$ [10,55] and $\lambda_b$ is assumed to be a small multiple, in the order of 10, of the mean dislocation spacing defined as $\frac{1}{\sqrt{\rho_m}}$ [56].

The corresponding range of DDL is then estimated from $\rho_m$ reported values to vary between $1.51 \bullet 10^{7}$ and $5.1 \bullet 10^{3}$. The resulting adjusting values for DDL obtained under the current modeling framework are presented in Table 3:

## 3. Results and discussion

### 3.1. GSFE as a function of temperature

Fig. 3.a presents the computed GSFEs for TiC and slip systems $\{110\} < 1\bar{1}0 >$, $\{111\} < 1\bar{1}0 >$and $\{111\} < 1\bar{2}1 >$at 0 K and 1000 K. Similarly, Fig. 3.b presents the corresponding GSFEs for VC. All curves are plotted in fractional coordinates such that the coordinate is normalized by the length of the perfect Burgers vector for slip in the $\{111\} < 1\bar{2}1 >$system ($3a/\sqrt{6}$). At 0 K, for both carbides, $\{110\} < 1\bar{1}0 >$is the slip system exhibiting a lower SFE, and therefore the easiest slip system to activate. The slip system showing higher SFE is $\{111\} < 1\bar{1}0 >$ and hence the least favourable. The slip of the crystal in the direction characteristic to partial dislocation gliding, $\{111\} < 1\bar{2}1 >$, exhibits an intermediate SFE at 0 K.

As temperature increases, the magnitude of all GSFE curves decreases. However, the extent of this decrease varies for different slip systems and materials. For both group IV and V carbides, the slip system that is affected the most by the increase of temperature (in magnitude and shape) is the slip in $\{111\} < 1\bar{2}1 >$. The fractional coordinate $^1/_3$ in this slip system is of particular interest because, due to the symmetry of the {111} plane, a local extremum is expected (point A in Fig. 3). For group IV carbides (TiC), ab initio calculations considering the contribution of harmonic phonons reveal an increased flatness of the SFE curve around this coordinate with increasing temperature. However, it is important to note that no local minimum is observed and therefore an ISF is not generated as an effect of the temperature. This finding contradicts the notion of partial splitting in group IV carbides. Nonetheless, Fig. 3.a shows that the SFE at point A $\{111\} < 1\bar{2}1 >$partial slip is considerably lower than that for $\{111\} < 1\bar{1}0 >$slip. Hence, slip motion through Shockley partials should be favorable on the {111} plane in TiC. In contrast, group V carbides (VC) exhibit an ISF at point A at 0 K. This ISF promotes partial splitting and is further enhanced when the rise of temperature deepens the SFE local minimum in point A. In the case of VC, the ISF configuration appears to be more stable than the B1 structure for temperatures above approximately 700 K (see Fig. 4.b). Consequently, at high temperatures, the deformation of VC may be governed by the formation of faults in conjunction with dislocation gliding. While the exploration of this mechanism is of interest for future investigations, it falls beyond the scope of the current research.

When analyzing point B in Fig. 3, corresponding to the fractional coordinate $^2/_3$ in $\{111\} < 1\bar{2}1 >$ slip system, it is clear how for both carbides the stacking of two metallic atoms, one above the other, results in very high SFE. As a result, the preferred slip should occur from point A to point C, rather than from A to B. For the case of TiC, temperature primarily reduces the magnitude of B while the condition of maximum is maintained. In contrast, VC tends to form a local minimum in point B as temperature increases. However, this minimum is surrounded by relatively high local maxima, suggesting that the slip from A to C remains preferred in VC.

The evolution with temperature of the characteristic points within the investigated slip systems can therefore provide some approximation on the energetically favored slip systems within different temperature ranges. Fig. 4.a shows the evolution of the SFE for $\{110\} < 1\bar{1}0 >$, $\{111\} < 1\bar{1}0 >$at half the slip, and for $\{111\} < 1\bar{2}1 >$at point A (Fig. 3) for TiC. As discussed, at 0 K, slip in {110} planes exhibits the lowest SFE, but from approximately $1000 \pm 100$ K the SFE for $\{111\} < 1\bar{2}1 >$partial gliding becomes lower. This is in good agreement with the classic mechanism considered to rule the B-D transition of TiC, in which slip in {111} is activated on behalf of {110} slip at temperatures around 1073 K [7,13,20,57,58]. Fig. 4.b presents analogous results for VC, indicating consistently lower energy for the ISF through the entire temperature range.

**Table 3**
Extreme values for testing and material conditions.

| Carbide | $\rho_m$ ($m^{-2}$) | DDL ($m^{-1}$) |
|---|---|---|
| TiC | $5.0 \bullet 10^{12}$ | $2.2 \bullet 10^{5}$ |
| VC | $7.0 \bullet 10^{12}$ | $2.7 \bullet 10^{5}$ |
| HfC | $2.3 \bullet 10^{16}$ | $1.5 \bullet 10^{7}$ |
| VC | $3.0 \bullet 10^{12}$ | $1.7 \bullet 10^{5}$ |
| NbC | $9.0 \bullet 10^{12}$ | $3.0 \bullet 10^{5}$ |
| TaC | $2.3 \bullet 10^{16}$ | $1.5 \bullet 10^{7}$ |

### 3.2. Core structure definition

A detailed study of the core structure of the strain-ruling dislocations provides significant insights into the deformation behavior of materials. Generally, the dislocation radius is narrower for stiffer materials and for smaller angles between the dislocation line and the burgers vector (screw dislocations). In the current work, dislocations have been considered as continuum objects that can be described using the P-N method and its subsequent model extensions.

The dislocation core radius can be determined in two ways: i) by using the analytical form of the P-N model with the restoring force assumed to be a sinusoidal function and ii) by approximating the dis-

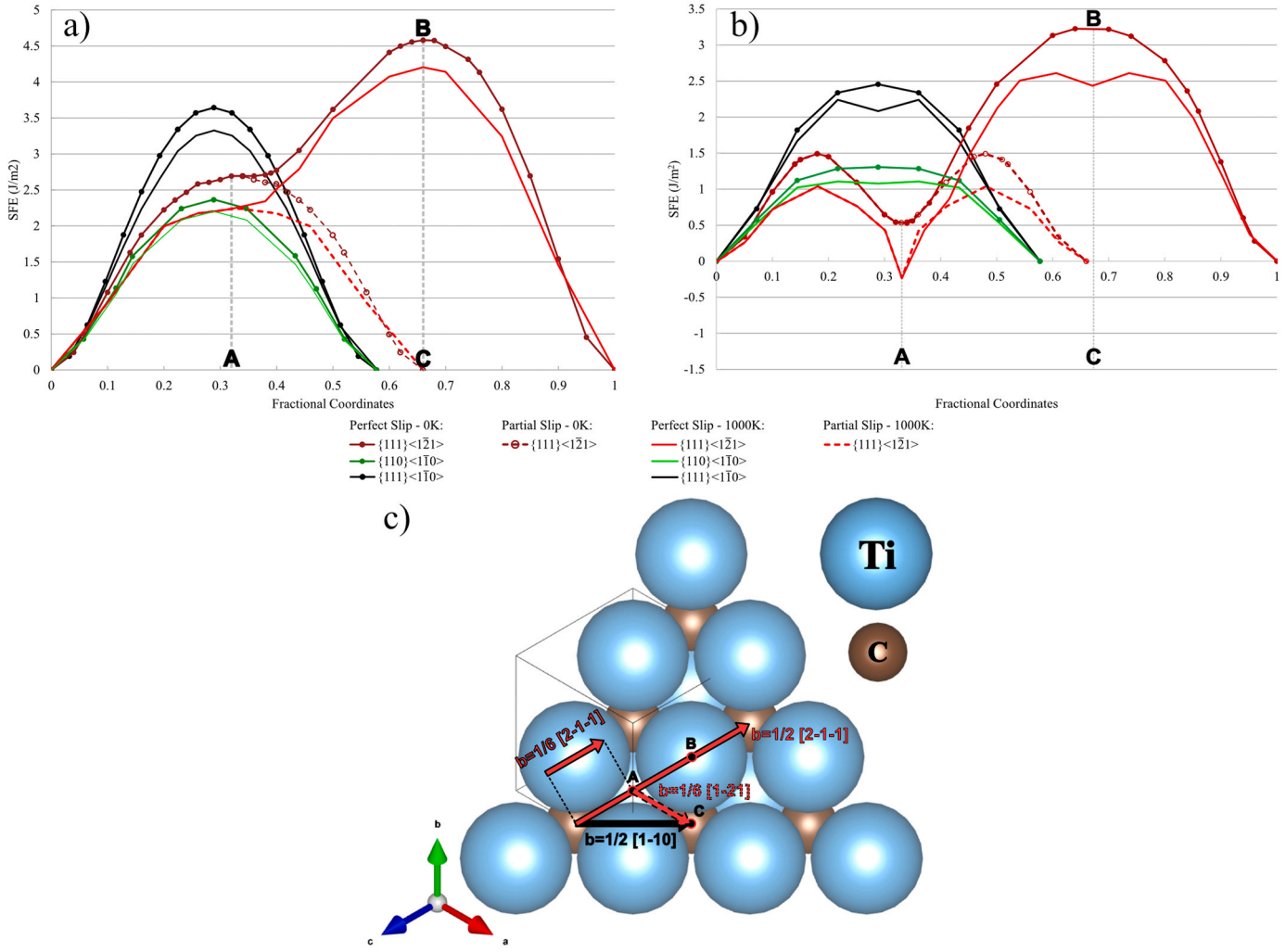


**Fig. 3.** Generalized stacking fault energies along $\{110\} < 1\bar{1}0 >, \{111\} < 1\bar{1}0 >$and $\{111\} < 1\bar{2}1 >$slip systems at 0 K and 1000 K. The coordinate is normalized by the length of three burgers vectors of the partials at $\{111\} < 1\bar{2}1 > (3a/\sqrt{6})$. a) TiC b)VC c) Atomic arrangement of the {111} plane in TiC with the relevant Burgers vectors depicted. (For interpretation of the color in this figure legend, the reader is referred to the web version of this article.) (2-column fitting image).

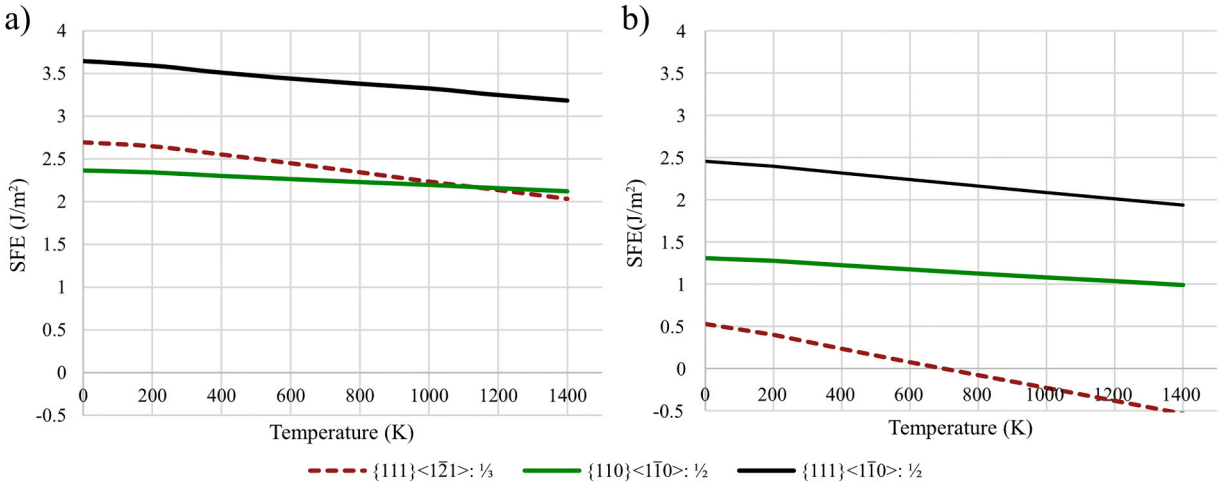


**Fig. 4.** Evolution of the SFE with temperature at half of the slip displacement for $\{110\} < 1\bar{1}0 >$, $\{111\} < 1\bar{1}0 >$slips, and for point A in $\{111\} < 1\bar{2}1 >$ slip in a) TiC b)VC. (For interpretation of the color in this figure legend, the reader is referred to the web version of this article.) (2-column fitting image).

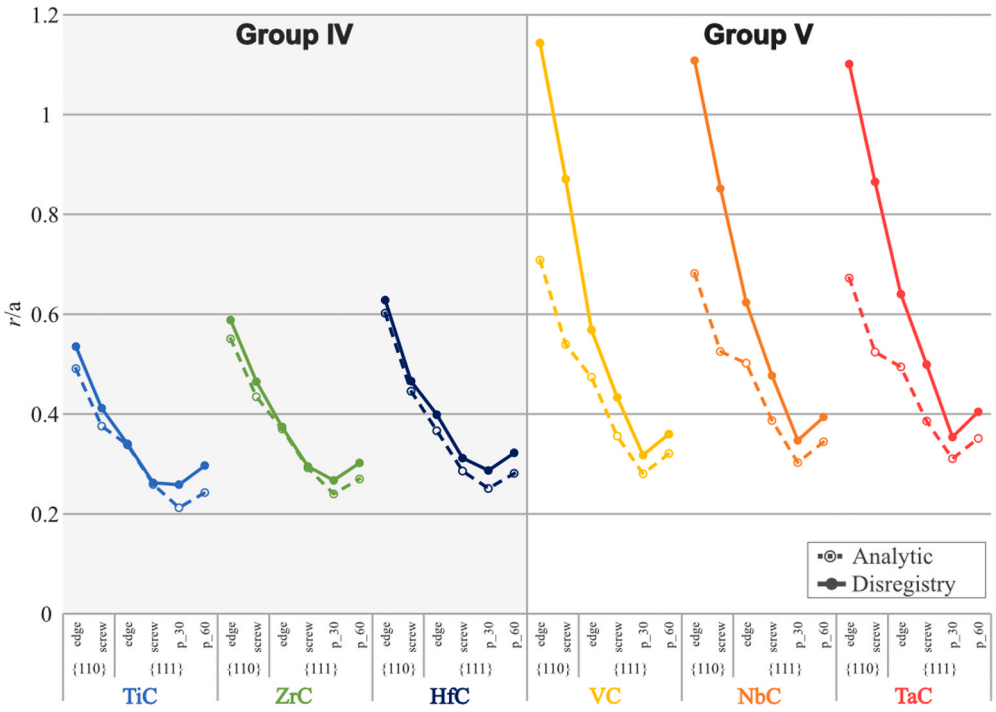


**Fig. 5.** Dislocation core radius normalized by the lattice parameter for all considered dislocations, defined through the analytical solution of the P-N model or through the disregistry fitted to an arctan series of order 6. (For interpretation of the color in this figure legend, the reader is referred to the web version of this article.) (1.5-column fitting image).

registry introduced by the dislocation by an arctan series up to an order of 6 [59], and the radius being defined as previously described. Fig. 5 depicts the results obtained using both methodologies for all considered TMCs at 0 K. As expected, for dislocations with the same Burgers vector, the larger the dislocation angle, the larger the dislocation core radius. For all group IV carbides, both methodologies lead to similar results. Whereas in group V carbides, the second methodology results in higher values for *r*. This is a direct consequence of group V carbides having a much flatter shape of the GSFE for the perfect dislocations glide in {111} and {110} planes, which leads to a broader spreading of the dislocation core. Therefore, when only the maximum SFE is considered (analytical method), the core radius is underestimated for group V carbides. Based on these results, the parameter *r* used in the hardness modeling has been defined using the values obtained from the Disregistry-based calculations. The values for *r* for all the considered dislocations obtained from this analysis, normalized by the lattice parameter of each carbide, are provided in Table 4.

Fig. 6 shows the fitted disregistries and dislocation densities, resulting from the disregistry-based methodology, for TiC and VC as representatives of group IV and group V carbides, respectively. The misfit density curves obtained for TiC present a monomodal dispersion of the misfit, indicating that none of the investigated slip systems exhibit a clear tendency towards dissociation of perfect dislocations into partials. On the other hand, $\{111\} < 1\bar{2}1 >$dislocations in VC are found to dissociate into two Shockley partials, both of which are identical and correspond to $\frac{a}{6} < 1\bar{2}1 >$. Furthermore, a partial splitting tendency is also observed in the $\{110\} < 1\bar{1}0 >$slip system for VC, where a strong overlap of both partials is observed. This trend is expected to be accentuated by temperature, as rising the temperature results in less directional atomic bonding [17]. This increase of partial splitting trend with decreasing atomic bonding directionality has been reported for group V carbides [26,60] when the nonmetal specie is changed from C to N. In these compounds the resultant change in valence electron charge (from 9 to 10) decreases the atomic bonding directionality and promotes the formation of an ISF that results in partial splitting of the dislocations in the $\{110\} < 1\bar{1}0 >$slip system.

The effect of temperature on dislocation splitting in TiC and VC can be seen in Fig. 7. The results indicate that an increase in temperature leads to modest increase of the core radius (Fig. 7.b and d), being higher for group V carbides. A stronger effect is observed in the trend towards partial splitting. In the case of TiC, this can be seen in the misfit density curves of the $\{111\} < 1\bar{2}1 >$dislocations in Fig. 7.a, which from 1000 K converge towards two separated peaks. This further confirms the increasing tendency of group IV carbides to deform through partial dislocation slip at higher temperatures. In the case of VC, the dislocations in $\{111\} < 1\bar{2}1 >$are already dissociated at 0 K and the increase of temperature just contributes to a larger separation.

**Table 4**
Cut-off radius normalized by the lattice parameter calculated at 0 K by means of 1-D Peierls-Nabarro calculation using PNADIS software.

| | | | | $\frac{r_{Cut-off}}{a}$ (@ 0 K) | | | | | |
|---|---|---|---|---|---|---|---|---|---|
| **Slip Plane** | **Slip Direction** | **Screw / Edge** | **β** | **TiC** | **ZrC** | **HfC** | **VC** | **NbC** | **TaC** |
| {1 1 0} | $\frac{1}{2} < 1\bar{1}0 >$ | S | 0° | 0.411 | 0.465 | 0.466 | 0.871 | 0.852 | 0.865 |
| | | E | 90° | 0.535 | 0.588 | 0.628 | 1.143 | 1.108 | 1.101 |
| {1 1 1} | $\frac{1}{2} < 1\bar{1}0 >$ | S | 0° | 0.262 | 0.295 | 0.311 | 0.433 | 0.477 | 0.499 |
| | | E | 90° | 0.340 | 0.374 | 0.399 | 0.569 | 0.624 | 0.640 |
| | $\frac{1}{6} < 1\bar{2}1 >$ | Mix | 30° | 0.259 | 0.267 | 0.287 | 0.318 | 0.347 | 0.354 |
| | | Mix | 60° | 0.297 | 0.302 | 0.322 | 0.360 | 0.393 | 0.404 |

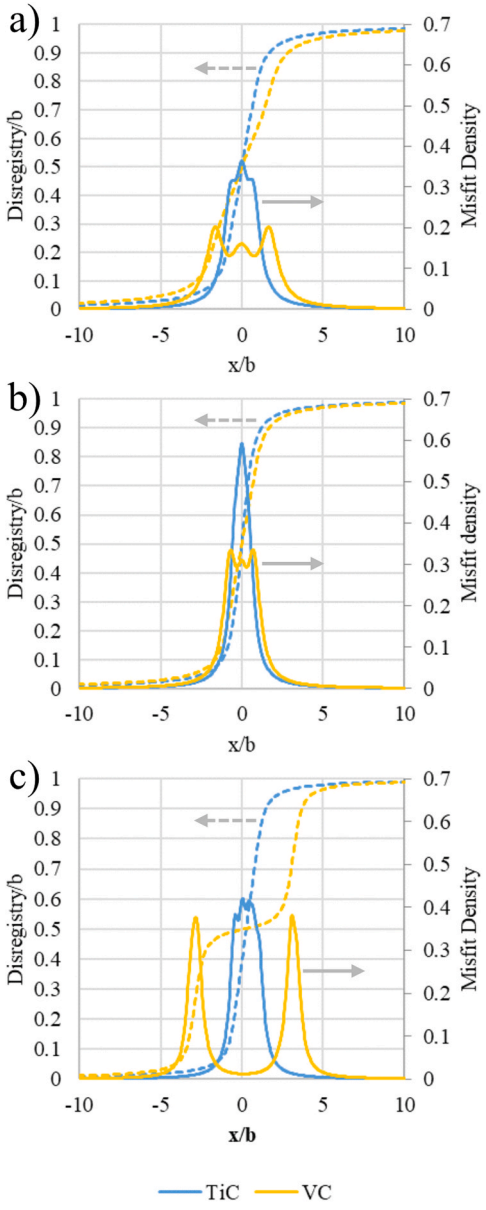


**Fig. 6.** Disregistry and misfit density of slip systems a) $\{110\} < 1\bar{1}0 > \beta = 90°$, b) $\{111\} < 1\bar{1}0 > \beta = 90°$, and c) $\{111\} < 1\bar{1}2 > \beta = 30°$ as a function of x/b of TiC and VC as representatives for group IV and V carbides respectively. (For interpretation of the color in this figure legend, the reader is referred to the web version of this article.) (single-column fitting image).

The change of the cut-off radius for dislocations of the $\{110\} < 1\bar{1}0 >$, $\{111\} < 1\bar{1}0 >$and $\{111\} < 1\bar{2}1 >$(i.e. Fig. 7.b and.d) slip systems with temperature have been calculated for TiC and VC and used for the calculation of the corresponding CRSS for group IV and V carbides respectively.

### 3.3. Hardness

Accurate calculation of hardness relies primarily on the correct determination of the CRSS required to move the dislocations. Therefore, the validation of the current model requires first to confirm that the CRSS as a function of temperature is accurately determined. Then the homogenous treatment of the Tabor and Schmid factors applied to the hardness of carbides, as well as the slip systems chosen to rule this property can be validated.

The slip system experimentally determined to be governing plasticity at homologous temperatures $> 0.3 \cdot Tm$ is $\{111\} < 1\bar{2}1 >$.The experimental CRSSs for this slip system for TiC [58,61–63], ZrC [64] and VC [65] are shown in Fig. 8 together with the calculated CRSS. The same trend and order of magnitude are obtained in both the calculations and the experimental measurements.

Fig. 9 presents the calculated hardness as a function of temperatures for group IV and group V TMCs. The hardness decreases with temperature for all carbides. The predicted values for hardness are in good agreement with the experimental measurements for TiC, ZrC, VC, and NbC. However, for TaC and HfC the predicted values tend to be slightly lower than experimental values at higher temperatures. This discrepancy may result from TaC and HfC being the carbides with largest metallic atoms, which impact the atomic bonding by enhancing its metallic character (as observed in the density of electronic states [26]. The calculated values for $\tau_{CRSS}$ and, therefore, for hardness are highly sensitive to the half width of the dislocation and to the periodicity of the crystal in the glide direction. In the current work, the dislocation core broadening for all carbides is for simplicity assumed to be the same as the one determined for TiC and for VC for all carbides of group IV and V, respectively. However, this broadening is expected to be larger the more metallic the bonding character is, thus, if higher precision was desired, the explicit calculation of the dislocation core properties for HfC and TaC should be considered.

A detailed examination of the CRSS calculated for each slip system can provide insights into the factors responsible for the softening of the materials. Fig. 10 presents the calculated CRSS for all slip systems and temperature ranges considered for all TMCs studied. The results show that the CRSS required for screw dislocations to move is considerably higher than that for edge dislocations, suggesting that most of the strain occurs through edge dislocation gliding. In group IV carbides, screw dislocations exhibit higher CRSS values across the entire temperature range compared to other slip systems. Conversely, in group V carbides, screw dislocations in the {110} planes have CRSS values in the same range as perfect and partial glide in the {111} plane, implying a possible source of cross-slip between these planes. This difference explains the experimentally higher ductility observed in group V carbides.

The slip system most affected by temperature is the one constituted by partial dislocations gliding in the {111} plane and, therefore, this is the primary contributor to the macroscopic softening of the material. This sharp decrease in CRSS also has a direct impact on the contribution of this slip system to the total slip. Fig. 11 illustrates the proportion of slip resulting from partial slip, determined using the weighting parameters specified in Eq. 13. The graph shows that the contribution of partial slip increases with temperature for all carbides. At low temperatures, Group V carbides exhibit a higher proportion of slip through perfect dislocations than group IV carbides in the {111} plane, primarily due to the former's lower and flatter generalized stacking fault energy (GSFE) curves. Within the same group, the presence of larger metallic atoms in the lattice promotes partial splitting, as evidenced by the increasing trends observed between TiC, ZrC, and HfC (being even more visible in group V carbides). In both groups, the proportion of slip attributed to partial slip becomes dominant (>0.5) from temperatures ranging from 0.2 to 0.3 $T_m$. This finding is consistent with experimental observations that report partial slip as the primary slip mechanism at high temperatures. Furthermore, these results align with recent findings [86] that employ similar modeling approaches, in conjunction with the Sachs model, to determine the contribution of each slip system to TMC high-temperature hardness.

### 3.4. Transition temperature

The precise temperature at which TMC present the B-D transition displays a wide range in literature [7,10,11,13,20,57,58]. However, a commonly accepted criterion is that TMCs undergo a change in their

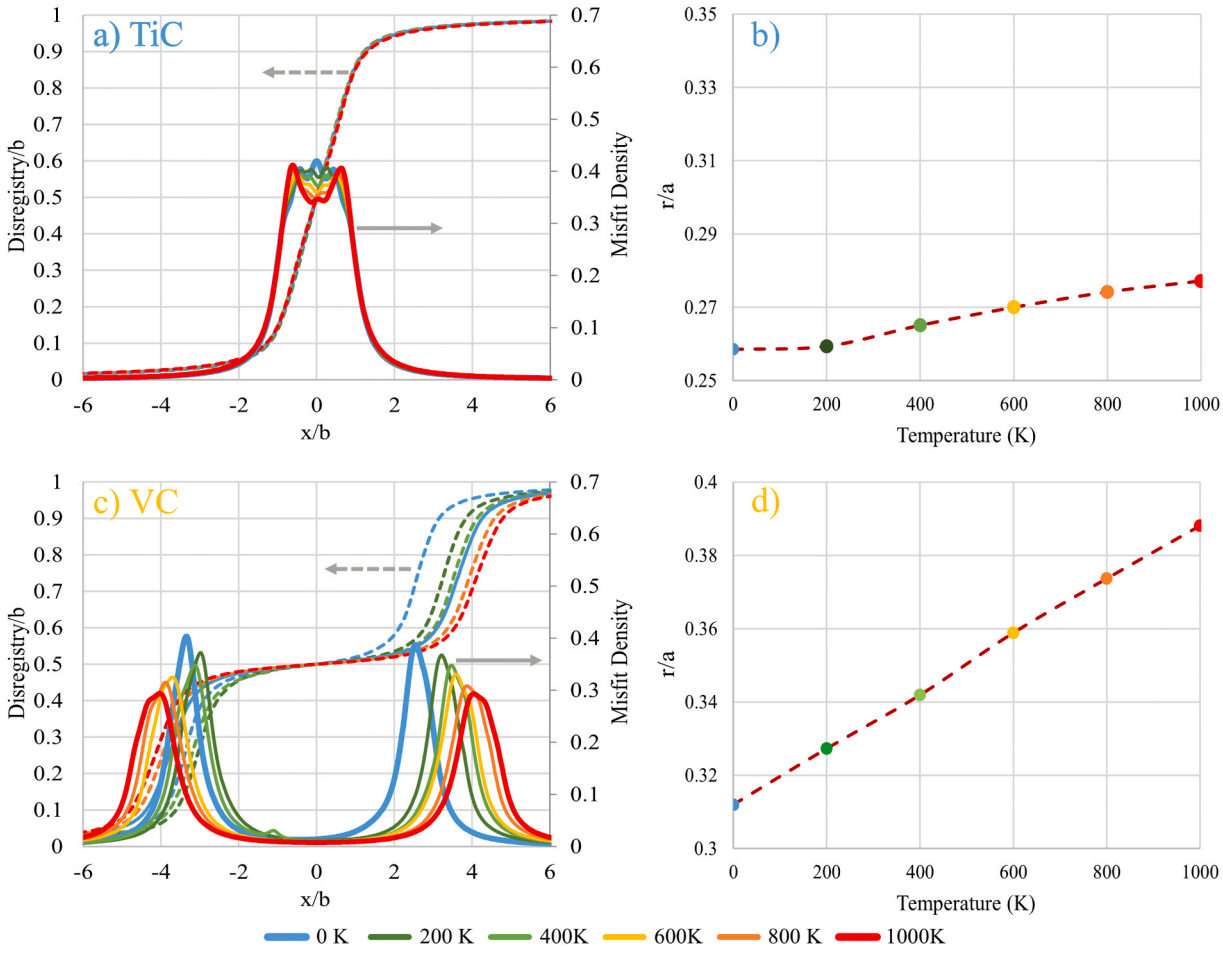


**Fig. 7.** a) Disregistry and misfit density and b) dislocation core radius as a function of temperature for TiC $\{111\} < 1\bar{2}1 >$slip system. c) Disregistry and misfit density and d) dislocation core radius as a function of temperature for VC $\{111\} < 1\bar{2}1 >$slip system. (For interpretation of the color in this figure legend, the reader is referred to the web version of this article.) (2-column fitting image).

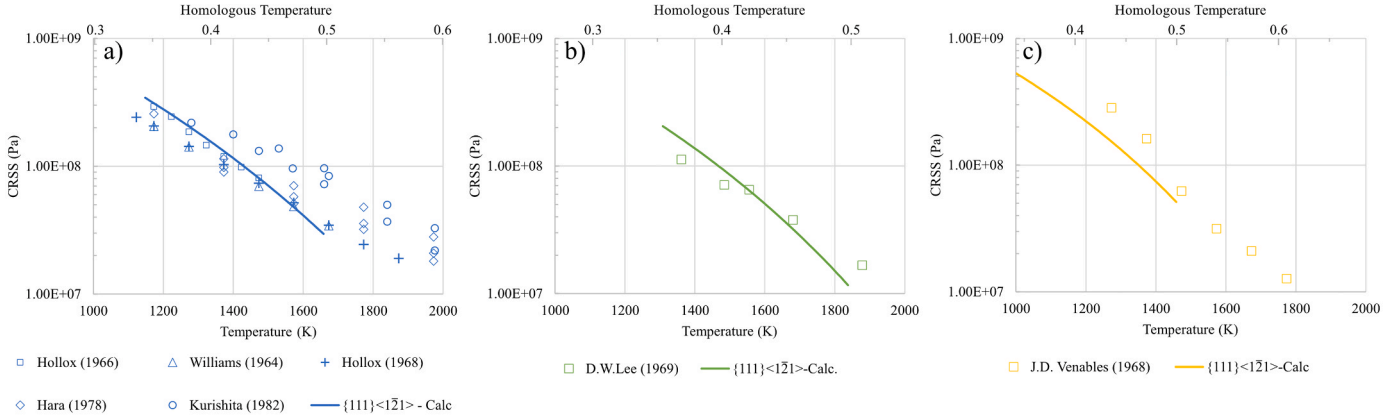


**Fig. 8.** Calculated and experimental CRSS for a)TiC [58,61–63], b)ZrC [64] and c) VC [65] (For interpretation of the color in this figure legend, the reader is referred to the web version of this article.) (2-column fitting image).

deformation mechanism when subjected to temperatures around 30% of their melting temperature, being the transition temperature higher the higher the strain rate is [20]. Considering a low temperature range far enough from the transition point i.e. $[0–0.15]\cdot T_m$, it can be assumed that TMCs ductility is ruled by a P-N mechanism. On the other hand, at medium temperatures below $0.5\cdot T_m$ (when creep diffusive mechanisms become relevant), the materials ductility is ruled by dislocation-dislocation interaction. A reasonable temperature range to assume that the material has already changed its mechanism is $[0.35–0.5]\cdot T_m$. This allows the B-D transition to be determined through a bilinear fitting of the predicted hardness, with one fitting range being $[0–0.15]\cdot T_m$ and the other being $[0.35–0.5]\cdot T_m$. The intersection point of the two trends can be considered to be the B-D transition temperature. The resulting construction applied to ZrC and NbC is shown in Fig. 12.b and d, respectively. It is evident from the plots that the assumption of hardness at both temperature ranges following two well-differentiated

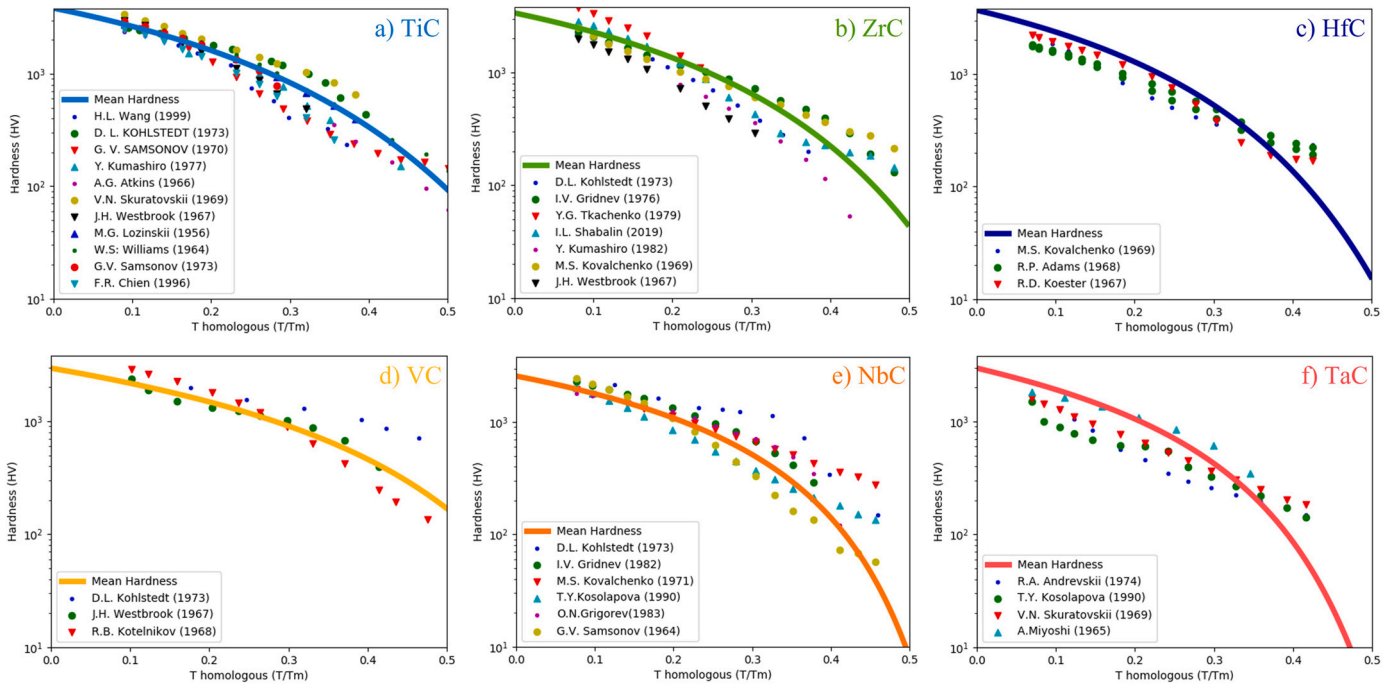


**Fig. 9.** Experimental and predicted hardness for a)TiC [4,7,8,19,61,66–70], b)ZrC [4,69,71–75], c)HfC [75–77], d)VC [4,69,78], e)NbC [4,79–83], and f)TaC [68,81, 84,85] (For interpretation of the color in this figure legend, the reader is referred to the web version of this article.) (2-column fitting image).

linear trends is realistic. This bilinear intersection method will be referred to as Method A henceforth.

The aforementioned works [20; 13; 10; 22] indicate that the activation of partial dislocations is of great significance for the B-D transition. In the case of group IV carbides, the CRSS for partial dislocation gliding in the {111} plane exhibits lower values than for perfect dislocation gliding in the {111} plane from temperatures as low as approximately 200–400 K (See Fig. 10.a,b,c and Fig. 12.c). Therefore, for TiC, ZrC and HfC, the B-D transition can be defined as the point at which CRSS for the partials become lower than that for perfect edge dislocation gliding on {110} planes. This intersecting point and its vicinity may be the region where dislocation climb from {110} to {111} planes occur. The high stacking fault energies in the carbides favor that the highly mobile dislocations present in the {110} plane start contributing to the slip in {111} planes, further softening the material. On the other hand, group V carbides present very low CRSS for {110} dislocation motion. Regarding the slip in {111} planes, the CRSS for perfect gliding is lower than that for partial gliding for a broader temperature range than in group IV. The B-D transition for VC, NbC and TaC can thus be defined as the temperature at which the CRSS for partial dislocation becomes lower than that for perfect edge dislocations in the {111} plane (See Fig. 12.e). The determination of B-D transition temperature from these intersecting points in the CRSS curves will be referred to as Method B.

Method B, provides a reference for the point at which both slip systems intersect. However, the overcoming of partial dislocations is expected to occur in a more diffuse nature in polycrystalline materials, where grains with different Schmid factors may present the activation of partials at a lower or higher temperature.

Fig. 12.a presents the B-D transition temperatures of all considered TMCs as determined by both Method A and Method B. The predicted transition temperatures were found to be in close proximity to the $0.3{\cdot}T_m$ threshold. Method A generally yielded transition temperatures that were closer to the theoretical values. On the other hand, Method B estimated the B-D transition temperatures to be close to the $0.3{\cdot}T_m$ approximation for all carbides except HfC and TaC. For these carbides, the predicted values were found to be underestimated.

## 4. Model assumptions and refinement opportunities

The hardness of group IV and V TMCs have been modeled as a function of temperature. However, the current model relies on certain assumptions that need further discussion.

a. Previous research has emphasized the significance of surpassing the {111} plane in relation to the {110} plane as the primary mechanism governing the B-D transition in TMC. While this can be of huge relevance in three-point bending or pure compression mechanical tests, this mechanism may not be as relevant when the high hydrostatic pressures present in hardness indentation, that inhibit the formation of cracks, are considered. Under hardness indentation testing, this change of slip system may not be observed, and the B-D transition is then determined by the thermal energy required to overcome the Peierls stress [7].

The current model assumes that partial dislocation slip is active throughout the entire temperature range for all carbide groups, including group IV carbides, which may be surprising given that they do not exhibit an ISF in their SFE curve at 0 K. The activation of one slip system over the other depends on a variety of experimental conditions beyond the strict activation energies determined from the crystal lattice's fundamental properties. Regarding the strain rate, in the current model a constant value of $10^{-3}$ is considered, but a gradient is expected within a single indentation, leading to several grades of severity in the microstructure. This difference between ideal modelling conditions and experiments, makes that even when not predicted from DFT calculations, the motion of partial dislocations in the {111} plane is observed at temperatures as low as 77 K for group IV carbides such as TiC or HfC [7,87,88].

Regarding the carbide's composition, current methodology considers perfect TMC crystals with a 1:1 C stoichiometry. However, it is well known that the depletion of C in group IV TMCs reduces the GSFE and therefore the CRSS required for slip to occur [89,90]. Nonetheless, experimental work on TMC presents some tolerance regarding its C:M ratio. Considering that the inflection point at 1/3 of the slip in the $\{111\} < 1\bar{2}1 >$already has a very flat profile in DFT

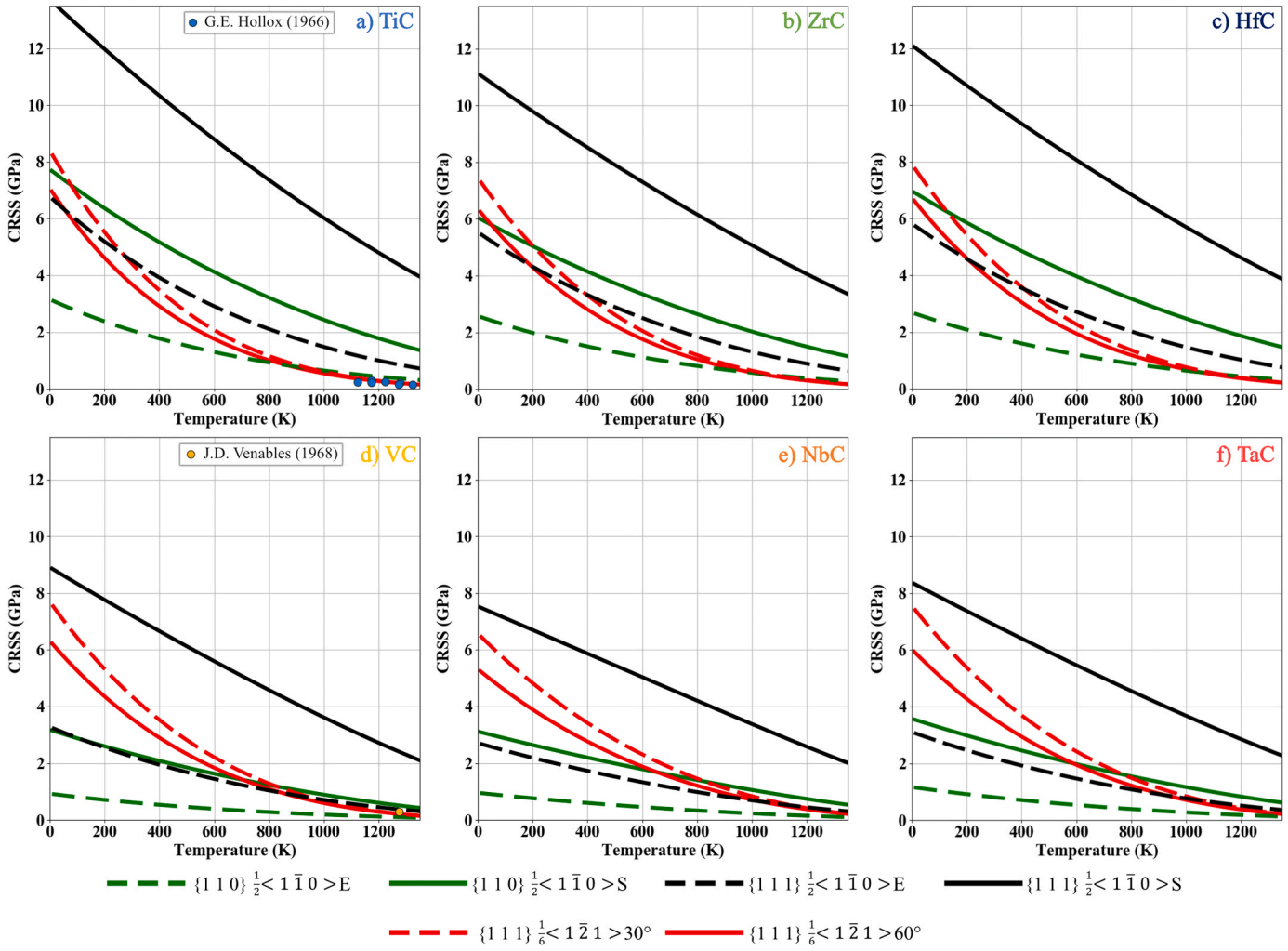


**Fig. 10.** CRSS calculated for a)TiC, b)ZrC, c)HfC, d)VC, e)NbC and f)TaC for all considered slip systems. (For interpretation of the color in this figure legend, the reader is referred to the web version of this article.) (2-column fitting image).

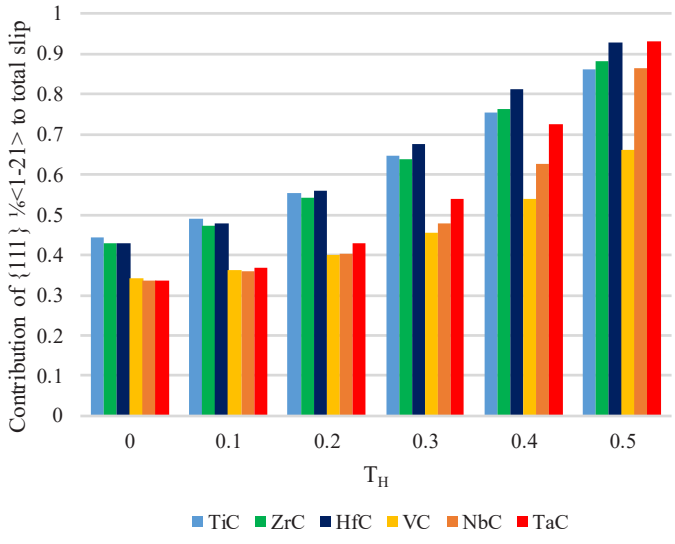


**Fig. 11.** Contribution of partial slip in the {111} plane to the total slip for every considered carbide as a function of their homologous temperature. (For interpretation of the color in this figure legend, the reader is referred to the web version of this article.) (1.5-column fitting image).

calculations that consider only temperature effect at the harmonic level. Physically, it is expected that chemical variations and additional effect of inharmonicities will promote partial splitting in group IV carbides.

In addition to the effect of under-stoichiometry, the presence of other transition metals in the carbide lattice can also influence dislocation splitting tendencies. For instance, TMC present in cemented carbides are often exposed to environments rich in W. DFT calculations have shown that the addition of V, W and Cr in order of relevance can decrease the total GSFE for slip and, more importantly, can cause an ISF in the GSFE curve in the $\{111\} < 1\bar{2}1 >$slip system. Therefore, when using models of TMC hardness to assess the intrinsic softening of γ-carbides present in cemented carbides, it is reasonable to assume partial splitting in the {111} plane from low temperatures.

b. The present study employs a simplified approach to evaluate the contribution of each slip system to the carbide's hardness. While this approach may oversimplify the problem at hand, the intermediate results generated from the present methodology can be used as input for more complex approaches such as crystal plasticity methods. These methods enable the calculation of the specific Schmid factor acting on each individual grain and plane with great precision.

Furthermore, the current model's averaging nature affects the predicted hardness by influencing the contribution of each slip system to the total macroscopic shear. It is common practice to assume that the slip system with the minimum shear stress exclusively

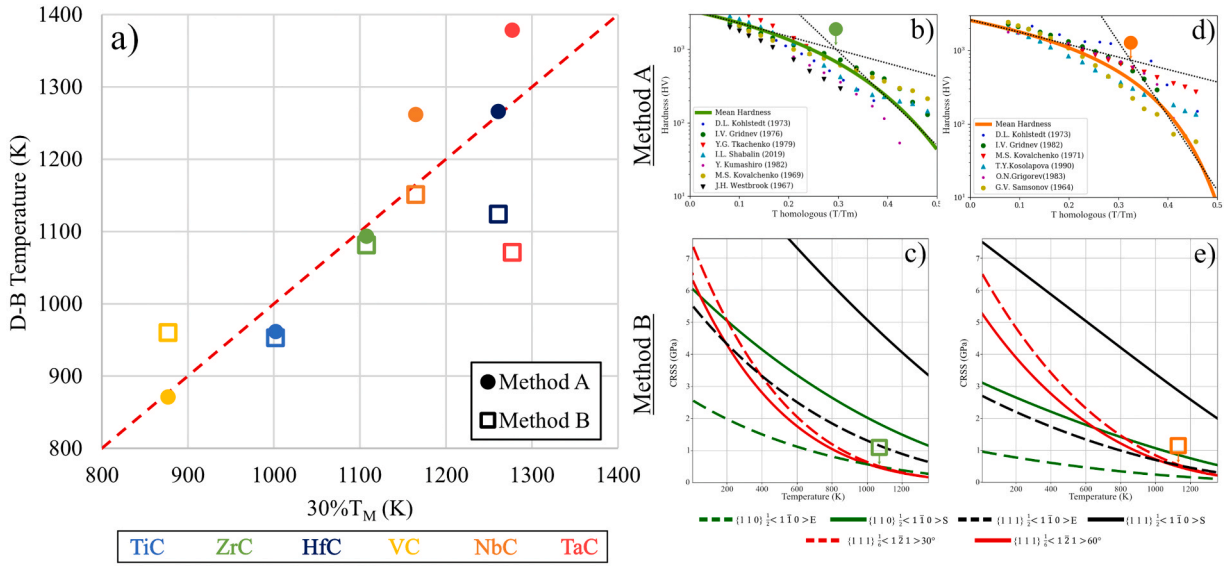


**Fig. 12.** a) Transition temperature for all considered TMCs determined through methodologies A and B. Schematic on how the transition temperature is determined through Method A and Method B for ZrC b) and c) and for NbC d) and e). (For interpretation of the color in this figure legend, the reader is referred to the web version of this article.) (2-column fitting image).

governs the material's mechanical behavior. However, this assumption is also considered to be a simplification. In regions where two slip systems have close CRSS, both slip systems can be activated. The model's good agreement with experimental data indicates that considering all possible slip systems contributing to shear, while accounting for a diffuse transition from one slip mechanism to another rather than a sharp change, enhances the hardness description.

c. The nucleation of kink-pairs for a dislocation to overcome a Peierls barrier of width *d* involves complex kinetics, which may benefit from a more sophisticated description. Currently, the kink-pair formalism is used across the entire temperature range up to $0.5 \cdot T_m$, serving as an upper limit for the dislocation mobility. This approximation is reasonable and its effect on the predicted hardness is expected to be subtle as the parameters affecting the dislocation kinetics are within the logarithmic term in Eq. 3. However, for temperatures exceeding $0.3 \cdot T_m$, where the thermally activated regime terminated, similar studies on MgO [6,91] indicate that the modeling of dislocation kinetics could benefit from the inclusion of Molecular Dynamics input or more complex definitions of the dislocations motion that consider possible backward and forward jumps.

Incorporating these additional components into the model would further improve the description of the mobility differences that screw, and edge dislocations exhibit in experiments, where long screw dislocations segments are visible at relatively low temperatures due to their low mobility. Edge dislocations show velocities between one and two orders of magnitude higher than screw dislocations [92]. In the present study, screw dislocations show very high CRSS that lead to a small contribution of these dislocations to the overall deformation. However, the physical reason for their low contribution is a combination of their high CRSS and their low mobility. Therefore, an improved description of this phenomenon would enhance the physical basis of the current modeling scheme.

d. The effect of experimental parameters such as the strain rate or the dislocation density could be studied using the current model. An increase of hardness with higher strain rates or lower dislocations densities is expected [86]. Nonetheless, determining a specific value for the dislocation density as a function of temperature and strain rate proves challenging. Thus, dislocation density is adopted as a fitting parameter. Still, the chosen dislocation density values are in good agreement with those reported in literature where they range among values of $10^{12} - 8 \bullet 10^{13}$ $m^{-2}$ for TiC [57,92], $9 \bullet 10^{13}$ $m^{-2}$ for HfC [16], and $10^{14}$ $m^{-2}$ for TaC and NbC [16,92].

## 5. Conclusions

In summary, a temperature-dependent Vickers hardness model was developed for closed packed refractory metal carbides using dislocation theory. The combination of P-N based models with DFT calculations proved useful in predicting macroscopic properties from mechanisms operating at lower scales. Because of this, the model not only predicts the material properties but also provides an understanding of the underlying mechanisms to a certain extent. It has been concluded that the slip in the {111} plane primary controls the Vickers hardness across the entire studied temperature range. At elevated temperatures, the hardness of these materials sharply decreases mainly due to two complementary factors. First, the increase in temperature promotes the splitting of perfect dislocations into partials for group IV carbides. Second, the CRSS required to move these dislocations decreases strongly with temperature.

This model relies on certain assumptions that make it useful for modeling the material properties without making the modeling process overly complex. The model could be used in good synergy with extended models [93,94] to describe the hardness-temperature dependance of cemented carbides. In this regard, the intrinsic softening of the hard phases is determined with the presented methodology and the specificities on the structure-properties relation derived from having a composite material are addressed with other methods. A critical point for the implementation of such a model in cemented carbides is the demonstration that the same scheme can be used for WC, the main carbide used in cemented carbides. WC possessing hexagonal-closed-packed crystallography, would require an exhaustive study of the relevant slip systems involved in its deformation.

Moreover, the proposed scheme can also be used in further complex modeling schemes, e.g., crystal plasticity modelling, that cover some of the assumptions made. The presented work can also be a base to include further parameters into the modeling of TMC mechanical properties such as the effect of substitutional dopants in high entropy alloys or more complex carbides or consider the effect of C vacancies (sub-stoichiometry or the carbides). In order to do so, recently reported first principles calculations of the SFE as a function of these parameters could

be included [89; 28]. In summary, this study offers valuable insights that can guide cemented carbide industry towards designing materials with a closer predictability in properties under service conditions.

## CRediT authorship contribution statement

**V. Lamelas:** Conceptualization, Methodology, Software, Investigation, Writing – original draft, Writing – review & editing, Visualization. **L. Tian:** Software, Data curation. **M. Bonvalet Rolland:** Conceptualization, Writing – review & editing, Supervision. **M. Walbrühl:** Supervision, Writing – review & editing. **R. Lizárraga:** Software, Writing – review & editing. **A. Borgenstam:** Supervision, Writing – review & editing, Funding acquisition.

## Declaration of Competing Interest

The authors declare that they have no known competing financial interests or personal relationships that could have appeared to influence the work reported in this paper.

## Data Availability

Data will be made available on request.

## Acknowledgements

The computations were enabled by resources provided by the National Academic Infrastructure for Supercomputing in Sweden (NAISS) and the Swedish National Infrastructure for Computing (SNIC) at the National Supercomputer Centre (NSC) in Linköping partially funded by the Swedish Research Council through grant agreements no. 2022-06725 and no. 2018–05973. R. L. and L. T acknowledge the Carl-Tryggers Stiftelse (CTS 22:2283).

## References

[1] D. Mari, Mechanical behavior of hardmetals at high temperature ([book auth.] V.K. Sarin). Comprehensive Hard Materials. s.l, Elsevier, 2014.
[2] High temperature deformation mechanisms in cemented carbides and cermets studied by mechanical spectroscopy K. Buss, D. Mari. 1-2, 163-167, s. l.: Mater. Sci. Eng. A Vol. 370 2004 doi: 10.1016/j.msea.2002.12.004.
[3] Influence of Cemented Carbide Composition on Cutting Temperatures and Corresponding Hot Hardnesses. al., A. Vornberger et. 4571, s.l.: Materials, 2020, Vol. 13.
[4] The temperature dependence of microhardness of the transition-metal carbides. Kohlstedt, D.L. 777–786, Cambridge: Journal of materials science, 1973, Vol. 8.
[5] Structural Ceramics. A.G. Evans, T.G. Langdon. 171-441, Thousand Oaks :Progress in Materials Science, 1976, Vol. 21.
[6] Modelling the rheology of MgO under Earth's mantle preassure, temperature and strain rates. Patrick Cordier, Jonathan Amodeo & Philippe Carrez. 177–179, Lille: Nature, 2012, Vol. 481.
[7] Slip systems and dislocation emission from crack tips in single crystal TiC at low temperatures. F.R.Chien, X.J.Ning, A.H.Heuer. 6, Cleveland: Acta Materialia, 1996, Vol. 44. 2265–2283.
[8] Hardness and Deformation Properties of Solids at Very High Temperatures. A.G. Atkins, D. Tabor. 1431:441–459, s.l.: Proceedings of the Royal Society of London. Series A, 1966, Vol. 292. ⟨https://www.jstor.org/stable/2415636⟩.
[9] Plastic flow and dislocation structures in tantalum carbide Deformation at low and intermediate homologous temperatures. C. Kim, G. Gottstein and D.S. Grummon. 7, East Lansing: Acta Metallurgica et Materialia, 1994, Vol. 42. 2291–2301.
[10] Chevacharoenkul, R.F. Davis. 2, Raleigh: Acta metallurgica, 1989, Vol. 37. 417–427'.
[11] The Ductile-BRittle transition in Tantalum Carbide. H.A. Johansen, J.G. Cleary. 4: 378–381, s.l.: Journal of the electrochemical SOciety, 1966, Vol. 133.
[12] Deformation of Poly crystalline Transition metal Carbides A. Kelly, D. J. Rowcliffe. 5: 253-256, s. l.: J. Am. Ceram. Soc. Vol. 50 1967 doi: 10.1111/j.1151-2916.1967.tb15098.x.
[13] Deformation behaviour of single crystals of titanium carbide. D.K. Chatterjee, M.G. Mendiratta, H.A. Lipsitt. 2151–2156, s.l.: Journal of Materials Science, 1979, Vol. 14. https://doi.org/10.1007/BF00688420.
[14] D.J. Rowcliffe, Plastic deformation of transition metal carbides ([book auth.] R.C. Bradt R.E. Tressler). Deformation of Ceramic Materials II, Plenum Press, New York, 1984.
[15] Independent slip systems in crystals G. W. Groves, A. Kelly. 89, 877-887, s. l.: Philos. Mag. Vol. 8 1963 doi: 10.1080/14786436308213843.
[16] Bonding effects on the Slip Differences in the B1 Monocarbides. al., Nicholas De Leon et. 165502, Tuscaloosa: Physical Review Letters, 2015, Vol. 114.
[17] Slip System determination in cubic carbides by hardness anisotropy. R.H.J. Hannik, D.L. Kohlstedt, M.J. Murray. 409–420, Cambridge: Proc. R. Soc. London A, 1972, Vol. 326.
[18] Anisotropy in the hardness of single crystals. C.A. Brookes, J.B.O'Neill, B.A.W. Redfer. 78–88, Exeter: Proc. Roy. Soc. Lond. A, 1971, Vol. 322.
[19] The micro-Vickers hardness of TiC single crystals up to 1500C. al., Y. Kumashiro et. 595–601, Tokyo: Journal of Material Science, 1977, Vol. 12.
[20] Hardness anisotropy, deformation MEchanisms and Brittle-to-ductile transition in carbides. D.J. Rowcliffe, G.E. Hollox. 1270–1276, Baden: Journal of Materials Science, 1971, Vol. 6.
[21] Plastic Flow and Fracture of Tantalum Carbides and Hafnium Carbide at Low Temperatures. D.J. Rowcliffe, G.E. Hollox. 1261–1269, Baden: Journal of materials Science, 1971, Vol. 6.
[22] Strength enhancement and slip behaviour of high-entropy carbide grains during micro-compression. al., Tamás Csanádi et. 10200, Kosice: Scientific Reports, 2019, Vol. 9.
[23] Nanomechanics of refractory transition-metal Carbides: a path to discovering plasticity in hard ceramics. al., Sara Kiani et. 8, Los Angeles: J. Am. Ceram. Soc., 2015, Vol. 98. 2313–2323.
[24] Phase, hardness, and deformation slip behavior in mixed HfxTa1-xC. al., Chase J. Smith et. 142–153, Tuscaloosa: Acta Materialia, 2018, Vol. 145.
[25] Dislocation core structures in titanium nitride. Salamania, J. Linköping: arXiv, 2022. 10.48550/ARXIV.2206.06222.
[26] Understanding dislocation slip in Stochiometric rocksalt transition metal carbides and nitrides. al., Hang Yu et. 6235–6248, Philadelphia: Journal Materials Science, 2017, Vol. 52.
[27] Origin of different plastic resistance of transition metal nitrides and carbides: Stiffer yet softer. R. Zhang, S. Sheng, S. Veprek. 12, Los Alamos: Scripta Materialia, 2013, Vol. 68. 913–916.
[28] Effect of transition metal atoms on the stacking fault energy and ductility of TiC. al., Yifan Li et. 29386–29391, Changsha: Ceramics international, 2021, Vol. 47.
[29] Universal scaling of the Temperature dependence of the strength of crystals governed by the Peierls mechanism. S. Takeuchi, T. Suzuki. 012014, Tokyo: Journal of Physicis: Conference Series, 2010, Vol. 240.
[30] Experimental evaluation of the Peierls stress in a variety of crystals and their relation to the crystal structure. Y. Kamimura, K. Edagawa, S.Takeuchi. 294–309, Tokyo: Acta Materialia, 2013, Vol. 61.
[31] J.P. Hirth, J. Loathe, Theory of Dislocations, John Wiley & Sons, New York, 1982. ISBN 0-89464-617-6.
[32] al., Wei Cai et. Chapter 64: Dislocation Core effects on Mobility. [book auth.] J.P. Hirth F.R.N. Nabarro. Dislocations in Solids vol.12. Livermore: Elsevier, 2004.
[33] Zur Kristallplastizität. I.I. Orowan, E. 614–633, s.l.: Z. Physik., 1934, Vol. 89. https://doi.org/10.1007/BF01341479.
[34] E. Schmid, W. Boas. Kristallplastizität: Mit Besonderer Berücksichtigung der Metalle. Berlin: Springer, 1935. 978–3-662–34261-9.
[35] The hardness of solids. Tabor, D. 145, Cambridge: Rev. Phys. Tech., 1970, Vol. 1.
[36] The correlation of indentation experiments Johns., K. L. 2, 115-126, s. L.: J. Mech. Phys. Solids Vol. 18 1970 doi: 10.1016/0022-5096(70)90029-3.
[37] The hardness of solids. Tabor, D. 145, Cambridge: Review of Physics in Technology, 1970, Vol. 1.
[38] Taylor Factors in materials with many deformation modes. H. Meckning, UF. Kocks, Ch. Hartig. 4: 465–471, s.l.: Acta MAterialia, 1995, Vol. 35. https://doi.org/10.1016/1359–6462(96)00137–6.
[39] Intrinsic stacking faults in body-centred cubic crystals Vítek, V. 154, 773-786, s. l.: Philos. Mag. A Vol. 18 1968 doi: 10.1080/14786436808227500.
[40] Phonons and related crystal properties from density-functional perturbation theory s. Baroni, s. de. Gironcoli, A. Dal Corso. 515-562, s. l.: Rev. Mod. Phys. Vol. 73 2001 doi: 10.1103/RevModPhys.73.515.
[41] Projector augmented-wave method Blöchl, P. E. 17953, s. l.: Phys. Rev. B Vol. 50 1994 doi: 10.1103/PhysRevB.50.17953.
[42] Gerenalized Gradient Approximation Made Simple. J. P. Perdew, K. Burke, M. Ernzerhof. 3865, s.l.: Phys. Rev. Lett., 1997, Vol. 77. https://doi.org/10.1103/PhysRevLett.77.3865.
[43] First-principles calculations of the ferroelastic transition between rutile-type and CaCl2-type SiO2 at high pressures. A. Togo, F. Oba, I. Tanaka. 134106, s.l.: Phys. Rev.B, 2008, Vol. 78. https://doi.org/10.1103/PhysRevB.78.134106.
[44] First principles phonon calculations in materials science A. Togo, I. Tanaka. 1-5, s. l.: Scr. Mater. Vol. 108 2015 doi: 10.1016/j.scriptamat.2015.07.021.
[45] Electronic and atomic structures of edge and screw dislocations in rock salt structured ionic crystals. al., Masaya Ukita et. 24, Nagoya: Philosophical MAgazine, 2018, Vol. 98. 2189–2204.
[46] Temperature-dependent elastic properties of binary and multicomponent high-entropy refractory carbides. Sangiovanni, D.G. 109634, Linköping: Materials and Design, 2021, Vol. 204.
[47] The Peierls Stress of Dislocations: An Analytic Formula. Duesbery, B. Joós and M. S. 266, s.l.: Phys. Rev. Lett., 1997, Vol. 78. https://doi.org/10.1103/PhysRevLett.78.266.
[48] Peierls-Nabarro model of dislocations in silicon with generalized stacking-fault restoring forces. B. Joós, Q. Ren, and M. S. Duesbery. 5890, s.l.: Phys. Rev. B, 1994, Vol. 50. https://doi.org/10.1103/PhysRevB.50.5890.
[49] PNADIS: An automated Peierls-Nabarro analyzer for dislocation core structure and slip resistance. S.H. Zhang, D.Legut, R.F. Zhang. 60–73, s.l.: Computer Physics Communications, 2019, Vol. 240. https://doi.org/10.1016/j.cpc.2019.03.005.

[50] Elastic moduli of niobium carbide and tantalum carbide at high temperature. C.K Jung, P.T.B. Shaffer. 367–373, Niagara falls: Journal of less-common metals, 1970, Vol. 23.
[51] Dynamic Indentation response of ZrHf-Based bulk metallic glasses. Ghatu Subhash, Hongwn Zhang. 2, Florida: Journal of materials research, 2007, Vol. 22. 478.
[52] Dynamic Vickers indentation of brittle materials. Richard J. Anton, Ghatu Subhash. 27–35, Houghton: Wear, 2000, Vol. 239.
[53] Grain size softening in nanocrystalline TiN. H. Conrad, J. Narayan, K. Jung. 301–305, s.l.: International Journal of Refractory Metals & Hard materials, 2005, Vol. 23. doi:10.1016/j.ijrmhm.2005.04.016.
[54] Calculations of thermophysical properties of cubic carbides and nitrides using Debye-Grüneisen model. X-G. Lu, M. Selleby, B. Sundman. 1215–1226, s.l.: Acta Materialia, 2007, Vol. 55. https://doi.org/10.1016/j.actamat.2006.05.054.
[55] How hard metal becomes soft: crystallographic analysis on the mechanical behavior of ultra-coarse cemented carbide. al., Huaxin Hu et. 1014–1023, s.l.: Acta Crystalographica B, 2019, Vol. 75. https://doi.org/10.1107/S2052520619013118.
[56] Dissemination of IT for the Promotion of Materials Science. Mechanisms of Plasticity. [Online] University of Cambridge, February 07, 2004–2023. [Cited: February 07, 2023.] ⟨https://www.doitpoms.ac.uk/tlplib/work_harden/printall.php⟩.
[57] Mechanical properties of polycristalline TiC. Das, G. 2: 104–110, s.l.: Journal of the American Ceramic Society, 1982, Vol. 65.
[58] Plastic behaviour of Titanium Carbide. Smallman, G.E. Hollox and R.E. 818, Edgbaston: Journal of Applyed physics, 1966, Vol. 37.
[59] Peierls-Nabarro model of dislocations in silicon with generalized stacking-fault restoring forces. B. Joós, Q. Ren, M. S. Duesbery. 5890, s.l.: Phys. Rev. B, 1994, Vol. 50. https://doi.org/10.1103/PhysRevB.50.5890.
[60] Plasticity mechanisms in HfC at elevated temperature and room temperature. Vinson, K.:34571, s.l.: Scientific Reports, 2016, Vol. 6. https://doi.org/10.1038/srep34571.
[61] Influence of Temperature, Strain Rate, Surface Condition, and Composition on the Plasticity of Transition-Metal Carbide Crystals. Williams, W.S. 1329, s.l.: Journal of Applied Physics, 1964, Vol. 35. https://doi.org/10.1063/1.1713614.
[62] High-temperature mechanical properties of titanium carbide. Hara, K., Yoshinaga, H., & Morozumi, S. 11: 1039–1047, s.l.: Journal of the Japan Institute of Metals, (1978), Vol. 42. https://doi.org/10.2320/jinstmet1952.42.11_1039.
[63] The High temperature deformation mechanism in titanium carbide single crystals. H. Kurishita, K. Nakajima, H. Yoshinaga. 2: 177–190, s.l.: Mat Sci Eng, (1982), Vol. 54. https://doi.org/10.1016/0025–5416(82)90112–4.
[64] Plasticity and Creep in Single Crystals of Zirconium Carbide D. W. Lee, J. s. Haggerty. 12: 641-647, s. l.: J. Am. Ceram. Soc. Vol. 52 1969 doi: 10.1111/j.1151-2916.1969.tb16067.x.
[65] (Structure of the ordered compound)J.D. V6C5 D. Venables Kahn R.G. Lye 151: 177-192, s.l Philos. Mag. Vol. 18 1968 doi: 10.1080/14786436808227320.
[66] Temperature dependence of ceramics hardness H. L. Wang, M. H. Hon. 3: 267-271, s. L.: Ceram. Int. Vol. 25 1999 doi: 10.1016/S0272-8842(98)00035-2.
[67] Temperature dependence of hardness of titanium carbide in the homogeneity range. Samsonov, G.V. 2: 327–331, s.l.: Phys. Stat. Sol. (a), 1970, Vol. 1. https://doi.org/10.1002/pssa.19700010217.
[68] A technique for the investigating the microhardness of refractory compounds within a wide temperature range. V.N. Skuratovskii, Yu.G. Tkachenko, V.A. Borisenko. 4: 393–396, s.l.: Strength Mater, 1969, Vol. 1.
[69] J.H. Westbrook, E.R. Stover, Carbides for high-temperature materials, pp. 312–348. [book auth.] E.M. Sherwood I.E. Campbell. High-temperature Materials and Technology, Wiley, New York, 1967.
[70] High thermal shock resistant indentors for the hardness measurement of metals at heating to 1300C in vacuum. M.G. Lozinskii, M.B. Guterman. 11:1358–1363, s.l.: Zavod Lab, 1956, Vol. 22.
[71] Effect of temperature on the strength characteristics of zirconium carbide. al., I.V. Gridneva et. 8: 638–634, s.l.: Powder Metall. MEt. Ceram., 1976, Vol. 15.
[72] Strength and anti-friction properties of alloys of the systems MIVC-MIVB2 over a wide range of component concentrations. al., Y.G. Tkachenko et. 4: 549–553, s.l.: Inorganic Materials, 1979, Vol. 15.
[73] Igor L. Shabalin, Zirconium Carbides. Ultra-High Temperature Materials II - Refractory Carbides I (Ta, Hf, Nb and Zr Carbides), Springer Nature, Singapore, 2019.
[74] The Vickers micro-hardness of NbC, ZrC and TaC single crystals up to 1500C. Y. Kumashiro, Y. Nagai, H. Kato. 2: 49–52, s.l.: J Mater Sci Lett, 1982, Vol. 1.
[75] Temperature dependence of teh hardness of titanium, zirconium and hafnium carbides. M.S. Kovalchenko, V.V. Dzhemelinskii, V.A. Borisenko. 5: 515–518, s.l.: Strength Mater, 1969, Vol. 1.
[76] R.P. Adams, Cast hafnium carbide- carbon alloys: preparation, evaluation and properties, Bureau of Mines, US department of teh interior, Washington DC, 1968. BM-RI-7137.
[77] Hot HArdness of selected borides, oxides and carbides to 1900C. R.D. Koester, D.P. Moak. 6: 290–296, s.l.: J American Ceram. Soc., 1967, Vol. 50.
[78] Osobo tugoplavkie element i soedineniya (Extra-refractory elements and compounds). al., R.B. Kotelnikov et. s.l.: Metallurgiya, 1968.
[79] Effect of temperature on the mechanism of failure and mechanical properties of niobium carbide single crystals. Gridneva, I.V. 5: 940–947, s.l.: Phys Met, 1982, Vol. 4.
[80] Microhardness of some carbides at various temperatures. al., M.S. Kovalchenko et. 8:665–668, s.l.: Powder Metall Met Ceram, 1971, Vol. 10.
[81] T.Ya Kosolapova, Handbook of High-temperature Compounds: Properties, Production and Applications, Hemisphere, New York, 1990.
[82] Influence of temperature on the failure of brittle materials in concentrated loading. O.N. Grigorev, V.I. Trefilov, A.M. Shatokhin. 12: 1028–1033, s.l.: Powder Metall Met Ceram 22, 1983, Vol. 22.
[83] G.V. Samsonov, Refractory Transition Metal Compounds, Academic Press, New York, 1964.
[84] R.A. Andrievskii, A.G. Lanin, G.A.Rymashevskii Prochnost, tugoplavkikh soedinenii (Strength of refractory compounds) (in Russian), Metallurgiya, Moscow, 1974.
[85] High temperature hardness of WC TiC TaC NbC and Their mixed carbides. A. Miyoshi, A. Hara. 2: 78–84, s.l.: Jap. Soc. Pow. and Pow. Met., 1965, Vol. 12.
[86] Temperature-dependent mechanical properties of TaC and HfC. all., Hailiang Liu et. s.l.: Journal of Materials Science, 2023, Vols. 58: 157–159. https://doi.org/10.1007/s10853–022-08026–6.
[87] Dislocation dissociation in Titanium Carbide Crystal. S. Tsurekawa, H. Yoshinaga. 4: 390–396, s.l.: J. Japan. Inst. Metals, 1994, Vol. 58.
[88] Evidence of dislocation dissociation in nearly stoichiometric tantalum carbide using the weak-beam technique. Martin, J.L. 2: 209–213, s.l.: Journal of Microscopy, 1973, Vol. 98.
[89] The influence of carbon vacancies on the stacking fault energy of TiC. al., Haimin Ding et. s.l.: Journal of the European Ceramic Society, 2014, Vols. 34: 1893–1897. https://doi.org/10.1016/j.jeurceramsoc.2014.01.013.
[90] Stacking Fault Energies in TiCx. R. Harris, P. Bristowe. 9, s.l.: MRS Online Proceedings Library (OPL), 1996, Vol. 458. doi:10.1557/PROC-458–9.
[91] Modeling the effect of preassure on the critical shear stress of MgO single crystals. J. Amodeo, P.Carrez, P. Cordier. 12, Lille: Pilosophical Magazine, 2012, Vol. 92. 1523–1541.
[92] R.F.. Davis et al., The ocurrence and behaviour of dislocations during plastic deformation of selected transition metal and silicon carbides. [book auth.] R.C. Bradt R.E. Tressler. Deformation of ceramic materials II. New York: Plennum Press, 1984.
[93] A model for the hardness of cemented carbides H. Engqvist, s. Jacobson, N. Axén. 384-393, s. l.: Wear Vol. 252 2002 doi: 10.1016/S0043-1648(01)00866-3.
[94] Hardness and Deformation of cemened tungsten carbide. H.C. Lee, J. Gurland. 125–133, s.l.: Materials Science and Engineering, 1978, Vol. 33. https://doi.org/10.1016/0025–5416(78)90163–5.